PARTICLE MANIPULATION USING MICROFLUIDICS

by

Kalpit Bakal

in partial fulfillment of the requirements for the degree of

Master of Science
in Mechanical Engineering

at the Delft University of Technology,

Student Number:	4739353
P&E Report Number:	2995
Supervisors:	Prof. dr. ir. Jerry Westerweel, TU Delft
	Dr. Daniel Tam, TU Delft
Daily Supervisor:	Ir. Ankur Kislaya, TU Delft
Thesis committee:	Dr. ir. Willem Haverkort, TU Delft

An electronic version of this thesis is available at http://repository.tudelft.nl/.

TU Delft Delft University of Technology

ACKNOWLEDGEMENT

I would like to thank **Prof dr. ir. Jerry Westerweel** and **Dr. Daniel Tam** for giving me this opportunity to work on this thesis. I would like to acknowledge the guidance I received throughout this thesis. I am deeply grateful to **Ankur Kislaya** for his supervision. Thank you for being available at all times for various discussions, taking into account my ideas and keeping me on track during the time of my thesis.

I would also like to thank **Edwin Overmars**, **Jasper Ruijgrok** and **Jan Graafland** for their support throughout the thesis. Special thanks to **Jan Graafland** for his help with LabView, without which it would not have been possible to capture images so efficiently. I am grateful to **Edwin Overmars** for his help with storing the experimental data and useful tips in postprocessing the same. I would like to thank **Tsun** for helping me 3D print the devices and **Dr. Burak Eral** for letting me use the Meth lab facilities.

A very special thanks to Udhav Gawandalkar for all the discussions: technical, philosophical, music and many more especially during our lunch breaks. You have been a good friend during this tough time of thesis. A special mention for Sudarshan Sridharan, Ankur Kislaya and Udhav Gawandalkar for the evening breaks. Furthermore, I would also like to thank all the PhDs and Post-docs for providing free coffee. I would also like to appreciate fellow Master students for making this time a little less stressful.

People who have been constant throughout my Master's programme: Mrigank, Afshan, Sawan, Neel and Priyanshi, thank you for being there in your own way. I cannot begin to describe each of your contributions since I have to limit this to a page. I would also like to thank Ketan, Sushobhan, Abhilasha and Surabhi for being there through telephonic conversations.

Last but not the least, a big thanks to **Aai** and **Baba**. This thesis would not have been possible without their constant support.

This thesis is dedicated to **Aaji** and **Amol Mama**. May their soul rest in peace

Kalpit Bakal
Delft, October 2019

ABSTRACT

The progress made by microfabrication technologies has escalated the interest in particle manipulation on micron scale. Particles are not only limited to solid particles but also include cells, droplets and bubbles. Activities involved in manipulation are trapping, sorting, separation and so on. The devices designed to execute such activities are aimed for a particular application. However, there lies a gap in literature to design a all-in-one device. Microfluidics research carried out at the Laboratory for Aero and Hydrodynamics is currently working on designing such devices which can carry out different manipulation tasks.

This thesis is aimed at designing and fabricating such a device where two particles can be manipulated simultaneously. The application of designing such a device would be to study cell-cell interaction, droplet coalescence and so on. To achieve this, a microfluidic device is designed as a Hele-Shaw flow cell. Since the height-averaged velocity in a Hele-Shaw flow cell is irrotational, analytical solution is possible for such a design. Although a Hele-Shaw flow is viscous flow between two closely spaced plates, it produces same streamline patterns as a 2D ideal flow. This enables the use of basic building blocks of an ideal flow field such as sources, sinks, uniform flow and so on. In this case, sources and sinks are superimposed to get the flow field inside the microfluidic device. The microfluidic device is fabricated using Polydimethylsiloxane (PDMS), a commonly used polymer to fabricate microfluidic devices. The design of the device is validated by comparing experimental flow fields, streamlines and stagnation points to the corresponding analytical solution. Single particle manipulation activities are carried out in the device. This is executed by manually controlling the flow rates or the strength of sources and sinks. Firstly, the particle is trapped at the stagnation point for a certain timespan. Finally, some manipulation activities are carried out using a single particle with the aid of streamlines produced by the sources and sinks.

Contents

LIST OF FIGURES

1

INTRODUCTION

The development of microfluidic devices has been on the rise lately due to their applications in medical and chemical industries. The major applications are related to manipulation and trapping of particles, cells, droplets and many more. The evolution of micro-fabrication technologies has further increased the pace of research in microfluidics. The small scale of the microfluidic devices requires lower sample volumes and allows cost-effective chemical and biological analysis.

Droplet coalescence studies in microfluidic devices such as selective droplet coalescence[6], geometrically controlled multi droplet coalescence[7] and electrically charged droplet coalescence [8] have been established. Research has been carried out to measure asphaltene content in oil to characterise the quality of oil [9] and also to measure equilibrium gas-oil ratio in live crude oil[10] using microfluidics. In medical field, tumor cells have been detected[11], isolated[12] and captured[13] using particle manipulation techniques. Separation of single cell from a cell suspension[14] and screening of single cells using droplet microfluidics[15] have also been undertaken. Particle assembly of micron sized non-spherical particles[16] and self assembly of particles[17][18] was carried out in microfluidic devices. All of the above mentioned studies use particle separation, trapping, sorting, filtering and so on to achieve various goals.

The above mentioned studies manipulates particles in two distinct ways: the active method, where external fields are used to control the motion of the particles and the passive method, which uses channel geometry and the flow field to manipulate particles. However, the active method relies on the physical properties of the particle to be manipulated whereas in passive method, the design of the channels varies depending on the application.

This thesis aims to manipulate particles using only flow fields without the use of real channels. First, design of the device is validated and then particle manipulation activities are carried out. The outline of the thesis is mentioned below.

1.1. OUTLINE OF THE REPORT

After a concise introduction to the topic, chapter 2 includes explanation of already existing manipulation techniques. The method used to design and fabricate the device along with the experimental setup is elucidated in Chapter 3. Validation of the design is shown in Chapter 4. Stagnation point manipulation and particle manipulation using unsteady fields are illustrated in Chapter 5.

2

State-of the art Particle Manipulation techniques

2.1. Introduction

Particle manipulation techniques are broadly divided into two categories, namely active and passive.Active manipulation is carried out on the basis of forces exerted by some external interface. This is achieved by using different force fields such as magnetic, optical and electrical. Magnetic forces were used in [11] to capture tumor cells. Electrical technique was used in sorting cells by marking them with polymeric bead[19]. Cell and molecule manipulation have been done by the use of optical tweezers [20].

Passive manipulation techniques use the drag force generated by different geometries in the microchannels. To cite a few, cancer cells have been isolated by steering them into different streamlines with the use of obstacles [21]. Continuous particle separation has been achieved using contraction or expansion in the microchannels [22].

In this project, particle manipulation will be done using only hydrodynamic forces. First, some history is briefly discussed relating to particle trapping. Furthermore, work already done on such flows will be discussed in detail.

2.1.1. History

Particle trapping was carried out on a macroscopic scale when G.I Taylor trapped a drop at the centre of the four-roll mill. The diameter of the cylindrical rollers were 3.81 cms and the height was 2.39 cms. The axles of these cylinders were fixed in the box of sides 7.6×7.6×3.9 cm. This apparatus was invented by G.I. Taylor to investigate deformation and subsequently bursting of a drop of one fluid in another. Before conducting the experiments, Taylor roughly estimated maximum size of the droplet that the surface tension might hold against the drag force. These estimates would just give an information about the deviation from the spherical shape of the droplet. Thus, experiments were undertaken to give an insight into the deformation of bubbles.

As can be seen from the figure 2.1, due to the extensional flow axis in the horizontal direction the drop was unstable and would move either in the left or right direction. This was controlled by controlling the speed of the right or left set of rollers. If the drop would move to the right, then the right set of rollers were retarded. However this was a complex task to control the rollers each time the drop would move away from the centre. Nearly five decades after the four-roll mill was introduced,

Bentley and Leal[2] controlled the rollers using a computer.

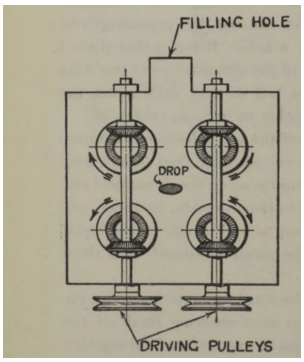

Figure 2.1: Four roll mill apparatus[1]

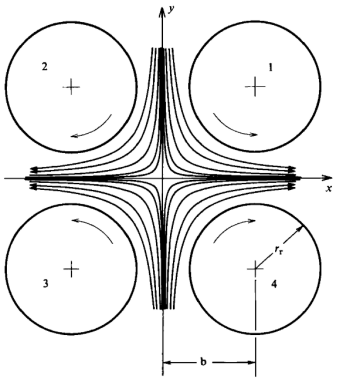

Figure 2.2: Schematic of a four roll mill(top view)[2]

The goal of this control was to keep the drop at the centre of the mill, where there is a stagnation point. Due to the addition of computer control to Taylor's four roll mill it became easier to control the rollers and study the droplet deformation.

The mention of history was done to show that stagnation point flow was used at a macroscopic level to study droplet deformation. Similar use of stagnation point flow was used in microfluidic devices to confine particles. There are several studies carried out in microfluidic devices using stagnation point flows. The concept used in such case is of a hydrodynamic trap explained in the next section.

2.2. HYDRODYNAMIC TRAP

As the name suggests the hydrodynamic trap uses hydrodynamic forces to confine particles and this approach can be divided into two categories: contact-based and non-contact methods[3]. Contact-based mechanism is based on placing obstacles of micron length scale, which efficiently traps a large number of particles[23]. An example of contact based method is the U-shaped hydrodynamic trap used for trapping single cells[24]. On the other hand, non-contact methods use stagnation point around the flows to confine particles without the use of obstacles.

Tanyeri et al[3] successfully confined one particle using a non-contact stagnation point flow. In this device, the horizontal axis is the compressional axis whereas the vertical axis is extensional. This can clearly be seen in figure 2.3. If the particle is to be confined along the compressional axis, it will experience a net attractive force towards the centre. Thus, being trapped at a stable equilibrium point. However, the stagnation point is an unstable equilibrium point along the extensional axis. Similar to the four-roll mill explained before, there lies a stagnation point at the centre of the device. The particle experiences no force at the center of the device as shown by particle 3 in figure 2.3(a). Also, it can be noted that the stagnation point can be moved along the extensional axis by adjusting the outflow conditions. This is displayed in figure 2.3 (b) and (c).

Shenoy et al [25] evaluated the trap performance with the aid of different control schemes and also conducted experiments, though only for single particle. They concluded that the integral control did not improve the performance of the trap whereas proportional control contributed to the improvement of trap performance and a particle could be confined for a longer time duration.

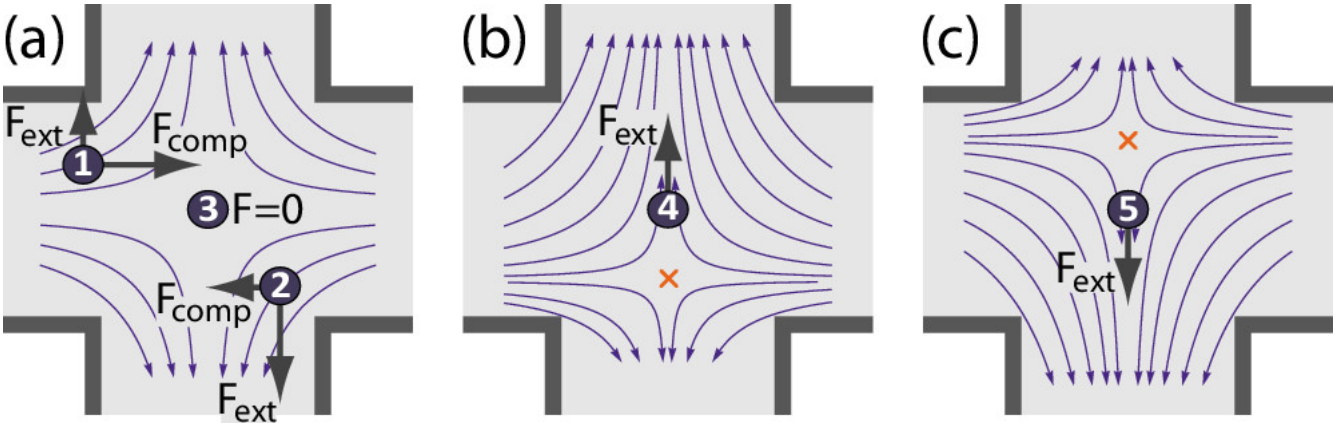

Figure 2.3: Flow in the cross slot device [3]

Until now, trapping of a single particle was studied. Schneider et al [26] laid the numerical framework for multi-particle manipulation using Hele-Shaw flow as a specific example. In their approach, they used the fact that the time dependent velocity field must satisfy the mass conservation(equation 2.1) and the Stokes equation(equation 2.2). Using the linearity of Stokes equation, it can be said that the velocity of the particles in the flow domain varies linearly with the boundary forcing (equation 2.3) [27]

$$\underline{\nabla}.\underline{v} = 0 \tag{2.1}$$

$$-\underline{\nabla}P + \mu\nabla^2\underline{v} + \rho\underline{b} = 0 \tag{2.2}$$

$$\underline{\underline{R}}(\underline{x})\underline{\dot{x}} = \underline{\underline{M}}(x).\underline{f} + \underline{F} \tag{2.3}$$

where:
$\underline{x} = [\vec{x}_1, \vec{x}_2, \vec{x}_3, ...\vec{x}_N]$ is the the position of N particles
$\underline{f}$ - flow rates of M inlets
$\underline{F}$ is the non-hydrodynamic interacting between particles
$\underline{\underline{M}}_{jk} = K_j(\vec{x}_1, \vec{x}_2, \vec{x}_3, ...\vec{x}_N; \xi_k)$,
$\underline{\underline{R}}$ and K_j depend on the geometry of the flow cell[28].

To get the flow rates for a given particle trajectory, the matrix M must be invertible. For that to happen, a necessary condition mentioned in [26] is that the number of independently controlled parameters must be greater than number of degrees of freedom. For a 2D domain, this implies that atleast 2N+1 inlets are required for N particles. But, the flow rates turn out to be too high for practical considerations. It was found that only 6 particles could be simultaneously controlled. To overcome this problem, sequential assembly of particles was carried out. As soon as two or more particles are attached to one another, they were treated as a rigid body and attempts were made to keep the center of mass of the aggregate at the center of the device.

2.3. STOKES TRAP

Shenoy et al [4] introduced a new method of trapping particles using fluid flow solely known as the Stokes trap. In this work, two particles were manipulated simultaneously using model predictive control. At low Reynolds number, Navier Stokes equation reduces to Stokes equation(equation 2.2): If H is the height of the device and if Hele-Shaw approximation is used, then the channel width

$W >> H$. The height averaged velocity inside the device can be written as-

$$\underline{v}(\underline{x}) = \frac{1}{\pi H} \sum_{i=1}^{N} \frac{(\underline{x} - \underline{R_i})}{||\underline{x} - \underline{R_i}||^2} . q_i \tag{2.4}$$

$$\sum_{i=1}^{N} q_i = 0 \tag{2.5}$$

Equation 2.4 represents velocity field due to N point sources in a 2D domain, where $\underline{R_i}$ represents the position of the i^{th} point source . It is possible to get the flow rates by inverting equations 2.4 and 2.5. But as mentioned in [26] that would give very high flow rates when two particles come close to each other. To avoid this control theory is used to get the flow rates.

As mentioned in [26], to control 2 particles in a 2D domain, atleast 6 point sources are required. Using this, Shenoy et al [4] fabricated a device with 6 channels with dimensions as shown in figure using soft-lithography technique and used MPC algorithm to successfully manipulate 2 particles simultaneously.

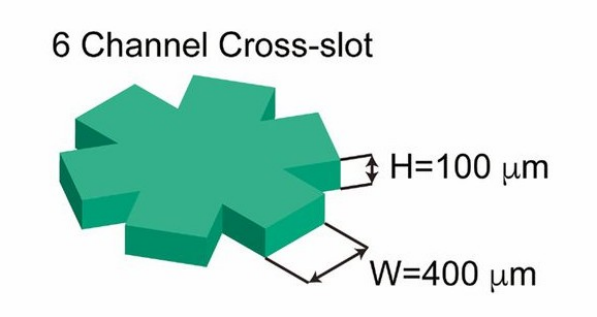

Figure 2.4: Schematic of device design used in [4]

2.4. APPROACH

In this thesis, particle manipulation is carried out with the use of sources and sinks. To achieve this, a device is designed based on the design used in [37]. The design of the device used stems from the fact that analytical solution can be used to solve for the velocity fields. Furthermore, the device design is validated by comparing experimental and analytical velocity fields. This project has the following research objectives:

- Design and fabricate a microfluidic device with sources and sinks to manipulate particles.
- Validating the device design by comparing experimental and analytical results.
- Moving the stagnation point quasi-steadily by changing the flow configuration.
- Introducing a particle inside the device and manipulating by using only sources and sinks.

3

DEVICE DESIGN AND EXPERIMENTAL SETUP

3.1. INTRODUCTION

Fabrication and validation of a suitable device is required to manipulate particles. A microfluidic design in a Hele-Shaw cell geometry is considered here. In this chapter, brief background theory related to Hele-Shaw flow, general information relating to the design of the device, the fabrication process and experimental setup is explained.

3.2. ANALYTICAL DESIGN OF FLOW DEVICE

Since Hele-Shaw flow cell is used, a description is given for the same before moving on to general design considerations. The streamline pattern generated by the Hele-Shaw flow is similar to 2D ideal flow. Therefore, a short description of ideal flow is also given in this section before describing Hele-Shaw flow.

3.2.1. IDEAL FLOW

Consider the figure 3.1, where velocities of two neighbouring points are represented. Using Taylor expansion of $\underline{\mathbf{u}}$ around $\underline{\mathbf{x}}$ gives [36]

$$du_i = \left(\frac{\partial u_i}{\partial x_j}\right) dx_i \tag{3.1}$$

$\frac{\partial u_i}{\partial x_j}$ is the velocity gradient tensor and can be split as follows (equation 3.2)

$$\frac{\partial u_i}{\partial x_j} = S_{ij} + \frac{1}{2} R_{ij} \tag{3.2}$$

where S_{ij} is the strain rate tensor and R_{ij} is the rotation tensor.The strain rate tensor represents the deformation of a fluid element as it translates whereas the rotation tensor represents the rotation of the fluid element as it translates. The individual elements of the rotation tensor can be represented by vorticity vector[36]. The rotation tensor then can be written as

$$R_{ij} = \begin{bmatrix} 0 & -\omega_3 & \omega_2 \\ \omega_3 & 0 & \omega_1 \\ -\omega_2 & -\omega_1 & 0 \end{bmatrix} \tag{3.3}$$

where,ω is the vorticity vector and can be represented as in equation 3.4

$$\underline{\omega} = \underline{\nabla} \times \underline{\mathbf{u}} \tag{3.4}$$

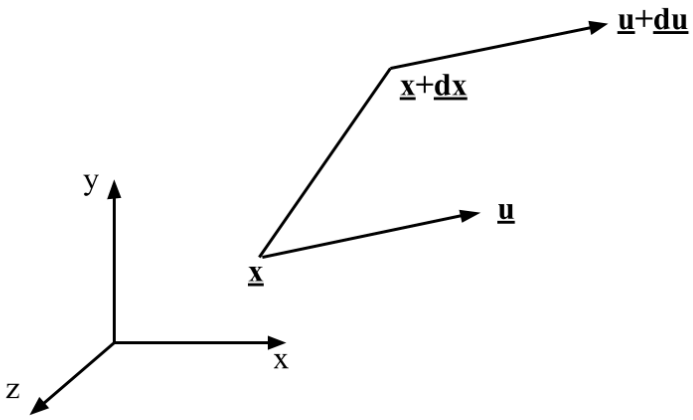

Figure 3.1: Velocity vectors **u** and **u+du** separated by a small distance **dx**

The absence of rotation in the fluid can characterise the flow and is called irrotational flow. The condition of irrotationality can be written as(equation 3.5):

$$\begin{aligned} \underline{\omega} &= 0 \\ \underline{\nabla} \times \underline{\mathbf{u}} &= 0 \end{aligned} \tag{3.5}$$

Since curl of a gradient is zero, velocity field can be defined as a curl of a scalar to satisfy equation 3.5

$$\underline{\mathbf{u}} = \frac{\partial \phi}{\partial \underline{\mathbf{x}}} \tag{3.6}$$

An incompressible, inviscid and irrotational flow is called an ideal flow. Buidling blocks of ideal flow such as sources, sinks, uniform flow can be superimposed to form myriads of flow patterns.

3.2.2. HELE-SHAW FLOW

Viscous flow between two parallel plates such that the length scales in the streamwise direction are large compared to the length scales in the wall normal direction is called a Hele-Shaw flow. Consider a Hele-Shaw flow in Cartesian coordinates as shown in figure 3.2. Furthermore, non-dimensionalising Navier-Stokes equation results in Stokes equation given the following conditions are met [36]:

$$\epsilon = \frac{h}{L} << 1 \tag{3.7}$$

$$\epsilon^2 Re_L << 1 \tag{3.8}$$

where, L is the streamwise length scale and h is wall normal length scale.

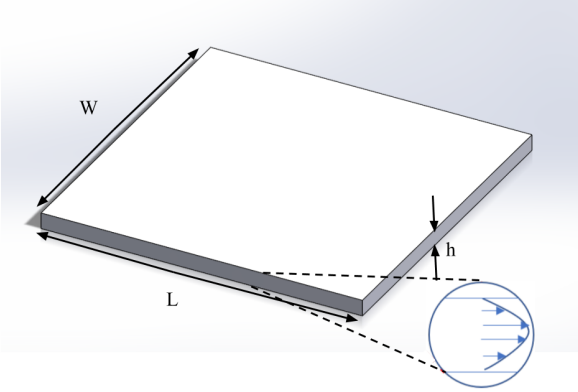

Figure 3.2: Schematic of a Hele-Shaw flow cell

The derivation for the velocity vectors are shown in appendix(put appendix name). The final result looks like

$$u = -\frac{1}{2\mu}\frac{\partial p}{\partial x}z(h-z) \tag{3.9}$$

$$v = -\frac{1}{2\mu}\frac{\partial p}{\partial y}z(h-z) \tag{3.10}$$

Integrating equations 3.9 and 3.10 over the height of the cell will give the height-averaged velocity.

$$u = -\frac{h^2}{12\mu}\frac{\partial p}{\partial x} \tag{3.11}$$

$$v = -\frac{h^2}{12\mu}\frac{\partial p}{\partial y} \tag{3.12}$$

The height-averaged velocity in both equations 3.11 and 3.12 is of the form $\underline{\mathbf{u}} = c\underline{\nabla}\phi$. This is similar to equation 3.6. This result is quite unexpected that viscous flow between two parallel plates produces same potential-lines as 2D ideal flow.. The height averaged Hele Shaw flow is irrotational and the proof can be found under the Lubrication theory section in book of Kundu[36]. In this case, the device is designed such that it is a Hele Shaw flow cell.

The device is designed similar to the design used in [37] shown in figure 3.3. Considering that the device is not only a Hele-Shaw flow cell but also circular in shape, condition for irrotationality (equation 3.13) in polar coordinates can be used.

$$\frac{\partial^2\psi}{\partial r^2} + \frac{1}{r}\frac{\partial\psi}{\partial r} + \frac{1}{r^2}\frac{\partial^2\psi}{\partial\theta^2} = 0 \tag{3.13}$$

The equation 3.13 represents that there is no vorticity component in the flow field. This equation is derived by considering the incompressibility condition followed by equating the vorticity to zero. The details of the derivation are mentioned in the book by Kundu [36].

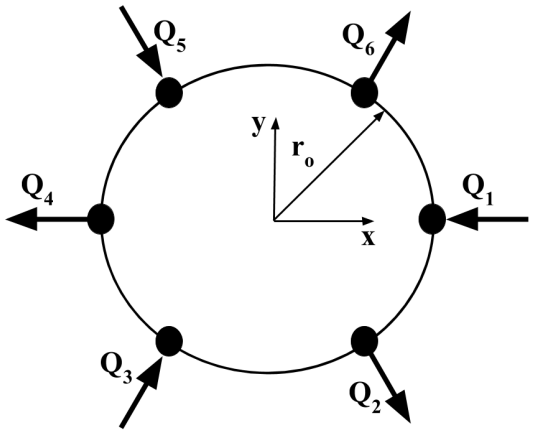

Figure 3.3: Schematic design of the microfluidic device

The design shown in 3.3 is chosen since the equation 3.13 can be used to solve for the flow field. Furthermore, there are advantages related to the device being symmetric. In figure 3.3 the arrows pointing inward towards the device is a source and the arrow pointing outward is a sink. Basic building blocks of potential flow (sources and sinks in this case) can be used since the height averaged flow is irrotational. In the figure3.3 Q represents the flow rate or the strength of sources and sinks. The reason for using 6 inlets/outlets is consistent with the condition mentioned in [26] for simultaneously manipulating 2 particles.

The boundary of the circular device is the streamline of the consecutive source sink pair and the boundary condition can be written as (equation 3.14)

$$\psi|_{r=r_0} = \sum_{i=1}^{6} Q_i H\left(\theta - \frac{(i-1)\pi}{3}\right) \tag{3.14}$$

where, θ is the angle made by the radial vector with the x axis in the counterclockwise direction, Q is the flow rate and $H(x)$ is the Heaviside function,

$$H(x) = \begin{cases} 1 & \text{if } x > 1 \\ 0.5 & \text{if } x = 0 \\ 0 & \text{if } x < 0 \end{cases}$$

Equation 3.13 can be solved subject to the boundary condition 3.14 to get the streamfunction. The steps involved are described in Appendix A. The final result for the streamfunction and velocity components are:

$$\psi = A_0 + \sum_{n=1}^{\infty} r^n [A_n \cos(n\theta) + B_n \sin(n\theta)] \tag{3.15}$$

$$A_0 = \frac{1}{6}\sum_{i=1}^{5} Q_i(6-i)$$

$$A_n = \frac{2}{r_0^n n\pi}\sum_{i=1}^{5} Q_i \sin(\frac{n(6-i)\pi}{6})\cos(\frac{n(4+i)\pi}{6})$$

$$B_n = \frac{2}{r_0^n n\pi}\sum_{i=1}^{5} Q_i \sin(\frac{n(6-i)\pi}{6})\sin(\frac{n(4+i)\pi}{6})$$

$$\boxed{v_r = \frac{1}{r}\frac{\partial \psi}{\partial \theta} = \sum_{n=1}^{\infty} n r^{n-1}\Big[-A_n \sin(n\theta) + B_n \cos(n\theta)\Big]} \tag{3.16}$$

$$\boxed{v_\theta = -\frac{\partial \psi}{\partial r} = -\sum_{n=1}^{\infty} n r^{n-1}\Big[A_n \cos(n\theta) + B_n \sin(n\theta)\Big]} \tag{3.17}$$

Equations 3.16 and 3.17 can be used to get the flow field inside the device. Qualitative results such as streamline plots can also be generated and compared to experimental results. However, it is necessary to design a practical device for experimental purposes.

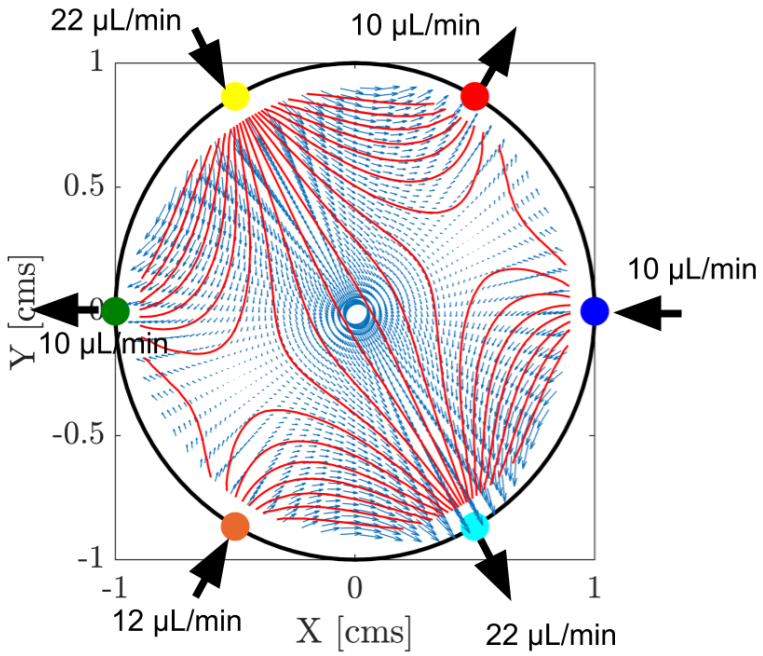

Figure 3.4: Velocity field and streamlines for given flow rate from equations 3.16, 3.17

Figure 3.4 shows the analytical plot for the velocity vectors and streamlines for the flow configuration mentioned in the figure. The equations used in this case were 3.15, 3.16 and 3.17

3.3. FABRICATION OF DEVICE

In microfluidics, the first step in fabricating the device is to design a mould which will be used to fabricate the device. In this case, the idea is to design the sources and sinks as channels. Therefore, the concept of hydraulic resistance plays an important role to decide the dimensions. A brief introduction to the concept of hydraulic resistance is given before moving on to the fabrication of device.

3.3.1. HYDRAULIC RESISTANCE

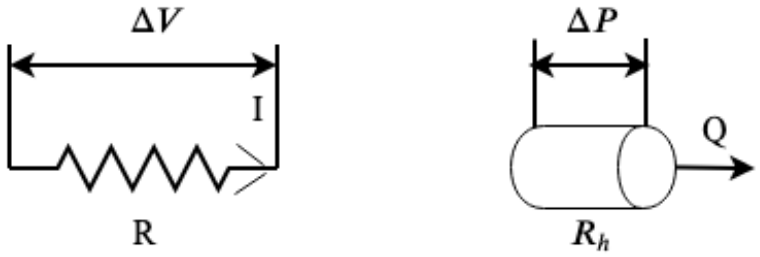

Figure 3.5: Wire with resistance and the corresponding Hydraulic resistance

For a steady Newtonian fluid flow through a tube, hydraulic resistance can be defined analogous to electrical resistance. Consider figure 3.5 which shows analogy between electrical and fluid system. Similar to Ohm's law where $R = \frac{\Delta V}{I}$, hydraulic resistance is defined as $R_h = \frac{\Delta P}{Q}$. For a Poiseulle flow, hydraulic resistance is defined as [38]

$$R_h = \frac{8\mu L}{A r_h^2} \tag{3.18}$$

where, L is the length of the tube, A is the cross section area of the tube and r_h is the hydraulic radius of the tube. $r_h = \frac{2A}{P}$, where A is the cross section area of the channel and P is the perimeter of the channel. The details for equation 3.18 can be found in the book by Kirby [38].

3.3.2. FABRICATION OF MICROFLUIDIC DEVICE

The sources and sinks shown in figure 3.3 are designed as channels. Based on the concept of hydraulic resistance, the dimensions of the channel are limited by the flow rate and pressure provided by the pump which is explained in detail in 3.4. The equivalent hydraulic resistance diagram is shown in figure 3.6b. The schematic design of the practical device is shown in figure 3.6a.

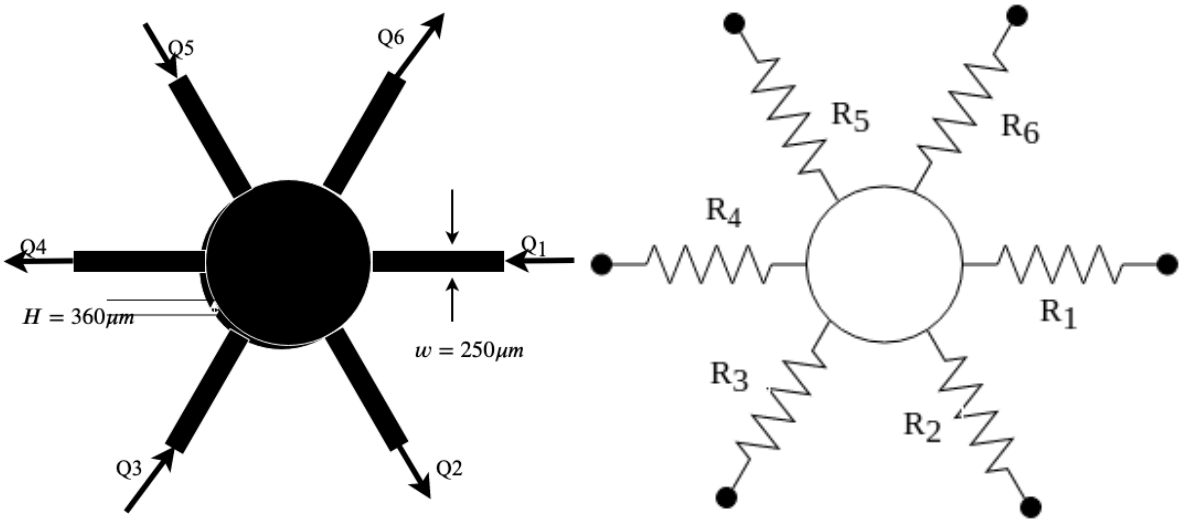

(a) Schematic design of the microfluidic device

(b) Equivalent hydraulic resistance diagram

Figure 3.6: Final design for the microfluidic device along with the hydraulic resistance circuit

In figure 3.6a, the sources and sinks shown in figure 3.3 are designed as channels. As can be seen in figure 3.6a the end of the channel opening in the circular chamber will act as the source or sink. The width 'w' should be kept as small as possible to ensure that the channels act as point sources/sinks. However, the smallest value that 'w' can go up to is determined by the size of particle (180μ m) to be manipulated. The height of the channel is decided based on the dimension of the particle (180 μ m) to be manipulated. After finalising the height and width of the device the length of the channel can be varied and is chosen using the concept of hydraulic resistance. The hydraulic resistance value should be such that the pressure values to achieve the prescribed flow rates should not exceed the capacity of the pressure pump being used. The limitations of the pressure pump and the flow rate sensor will be explained in detail in section 3.4

After finalising the design of the device, $SOLIDWORKS^{TM}$ is used to design the mould. The mould is then 3D printed as shown in figure 3.7 . Since, Polydimethylsiloxane (PDMS) is used to fabricate the microfluidic device, the 3D printed mould needs to be hydrophobized using 'TRICHLORO(1H,1H,2H,2H-PERFLUOROOCTYL)-SI' under 100 mbar pressure. This is done to ensure the ease while peeling the PDMS off the mould.

After hydrophobizing the device, PDMS samples are prepared using 1 gram of curing agent for every 7 grams of base. The prepared sample is then mixed using a spatula until the mixture turns opaque due to air bubbles. This mixture is centrifuged at 7400 rpm for 15 minutes to get rid of the dust particles and poured on the 3D printed mould placed in a glass petri dish. The petri dish is placed in a vacuum chamber and is desiccated to remove the air bubbles. The petri dish is then placed in the oven and heated overnight at 65^oC. On the next day, take the petri dish out of the oven, use a scalpel to cut the device off the mould. To make holes for the inlets/outlet use the surgical puncher as shown in figure 3.8. Once the device is ready sonicate it in the ultrasonic bath with ethanol for 10-15 minutes. This will remove any dust particles present in the device.

The next step is to bond this PDMS device to the glass slide. The first step is to make a PDMS sample with 10 grams of base for every 1 gram of curing agent. Mix the sample well with a spatula until the sample appears opaque due to air bubbles. To get rid of the bubbles and the dust centrifuge the sample at 7400 RPM for 15 minutes. Before pouring the PDMS on the glass slide, clean the glass slide with ethanol/methanol. Using a syringe, take 5ml of the PDMS sample and inject it on the glass slide ensuring there are no bubbles on the surface. A spincoater with in-house settings is used to uniformly spread the PDMS on the glass slide. The glass slides are then placed on an aluminium foil in a petri dish followed by placing the petri dish in the oven at 65^oC. The glass slides are checked periodically to ensure if the PDMS has semi-cured. The cut PDMS devices are then bonded to the glass slide ensuring that it sticks well from all sides. These bonded PDMS devices are then placed overnight in the oven at 65^oC. The final device looks like the one shown in figure 3.9.

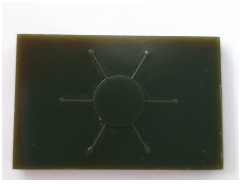

Figure 3.7: 3D printed mould

Figure 3.8: PDMS puncher

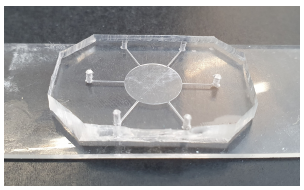

Figure 3.9: Device after bonding to the glass slide

3.4. EXPERIMENTAL SETUP

The overview of experimental setup is shown in the figure 3.10. The components of the setup will be explained in detail in this section. The experimental setup consists of the following

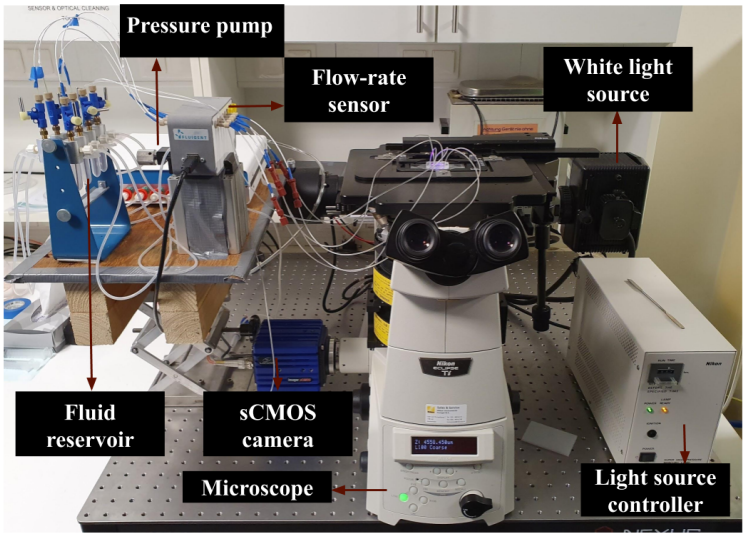

Figure 3.10: Experimental Setup

- **Pressure Pump**: The pressure pump (MFCS EZ) provided by FLUIGENT consists of 8 pressure ports and is driven by a nitrogen cylinder. The digital reading highlighted in green in figure 3.11 shows the pressure delivered from the nitrogen cylinder to the pressure pump in mbar. The ports highlighted in red can go upto a maximum pressure of 69 mbar and the ports in blue can go upto a pressure of 345 mbar. The pressure in each ports can be controlled with the aid of FLUIGENT A-i-O (All-in-One) software. In this project 6 out of the 8 pressure ports are used.

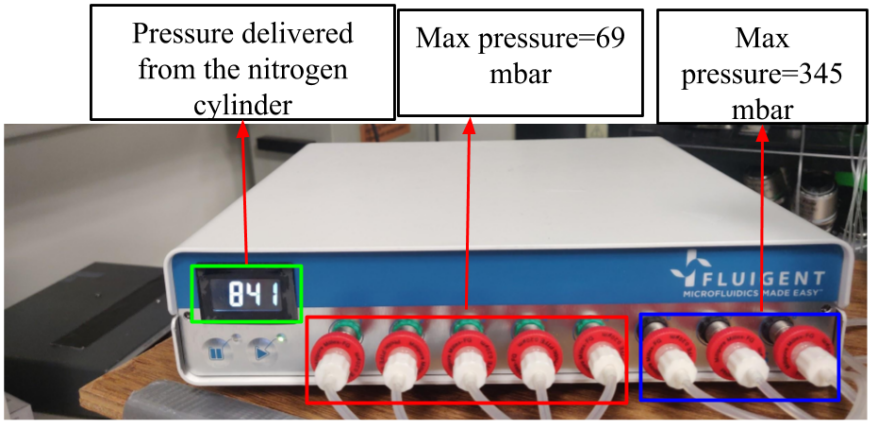

Figure 3.11: Pressure Pump

- **Flow rate sensor**: Flow rate platform supplied by FLUIGENT measures the flow rate through each port. The sensor has a capillary inside through which the fluid flows. This capillary is heated by a microheater by a temperature of around 1^{o}C. The two temperature sensors are placed at the inlet and outlet of the capillary and the flow rate is calculated by the distribution

of heat. A detailed explanation is provided in [5]. The flow rates can be manipulated using A-i-O software. 5 out of the 8 flow ports are used in this project. Please note that although 6 pressure ports are used, 1 of the tubings is not connected to the flow port and is directly connected to either of the sinks in figure 3.6a.

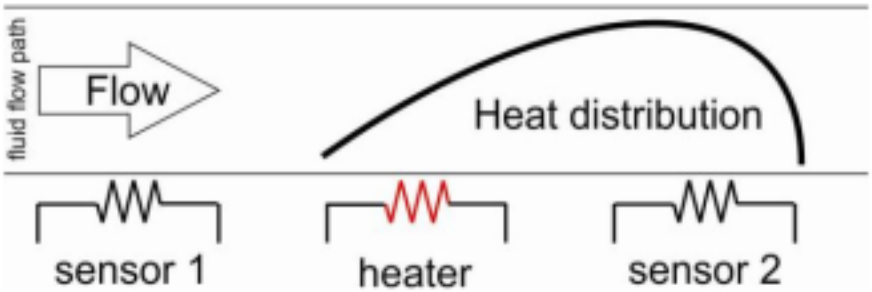

Figure 3.12: Principle behind working of flow sensor([5])

- **Microscope**: The Nikon Ti microscope is equipped with lenses of varying magnifications and numerical apertures. 1x magnification is used in this project.
- **Light source**: Mercury lamp is used as a white light source to illuminate the measurement volume for conducting volume illuminated Particle Image Velocimetry (PIV) studies. A purple filter is places such that the light that reaches the volume of interest is purple in colour.
- **Camera**: A sCMOS camera is attached to the left of the microscope as can be seen in figure 3.10. The microscope can be set so that 100% of the light scattered from particles in the volume illuminated zone is captured by the camera. A red filter is placed in front of the camera such that only red light reaches the camera. The maximum acquisition of the camera is 50 Hz.
- **Reservoirs**: A reservoir is used to store the fluid which will be pumped in the microfluidic device. The capacity of the reservoir is 2ml.
- **Tubings**: Three types of tubings are used
  - PEEK tubing inside the reservoir with inner diameter 0.5mm and outer diameter of 1.6 mm
  - PEEK tubing of inner diameter 0.5mm and outer diameter 0.8mm starting from the reservoir and passing through the flow rate sensor
  - PTFE tubing of outer diameter 1.6mm and inner diameter 0.8mm connects the end of PEEK tubing from the flow rate sensor to the device.

The nitrogen cylinder drives the pressure pump,which creates pressure in the fluid reservoir. The fluid rises through the tubes and goes through the flow sensor, which shows the flow rate reading in μ L/min. The tubings coming out from the flow sensor are connected to the device. Fluorescent orange particles of diameter 20-27 μm and density of 1.002 g/cc are used for seeding the flow. The light scattered by these particles is captured by the camera.

The fluorescent orange tracer particles used for doing Particle Image Velocimetry (PIV) studies are surface treated with Tween 20 solution so that they do not stick to each other. First a container is filled with distilled water and is boiled. Furthermore, 0.1g of Tween 20 per 100 ml of water is weighed and slowly added to the boiled water while mixing. A desired amount of particles is placed

in a container and the prepared tween solution is dispensed over the particles. This solution is centrifuged for 5-10 minutes until all the particles are not floating on the surface. These surface treated particles are then added to a fixed volume of DEMI water such that the solution appears concentrated with particles.

4

STUDY OF STEADY FIELDS

The first step after designing and fabricating the device is to validate the design. Experiments are conducted on the fabricated device and the results are compared qualitatively to its analytical counterpart. Later the ratio of the flow rates is reduced and the streamline patterns are observed again.

4.1. DESIGN VALIDATION

As can be seen from figures 3.3 and 3.6a the microfluidic device is symmetric. The sources and sinks are placed in an alternating way. This gives rise to an interesting case of equal magnitude of flow rates in all the channels. Figure 4.1a shows analytical result and figure 4.1b represents experimental results for the flow rate values mentioned in 4.1b. The arrow pointing towards and inside the device is the source and other is the sink, with flow rate values mentioned with the units. The sources and sinks are colour coded in both the figures. The point marked with magenta inside the device is the stagnation point. The curves represented by black in figure 4.1a are the streamlines and are represented by white in figure 4.1b. The same explanation holds for figures 4.1e, 4.1f, 4.1c and 4.1d. The streamline pattern and the stagnation point from both analytical and experimental results seem to match well.

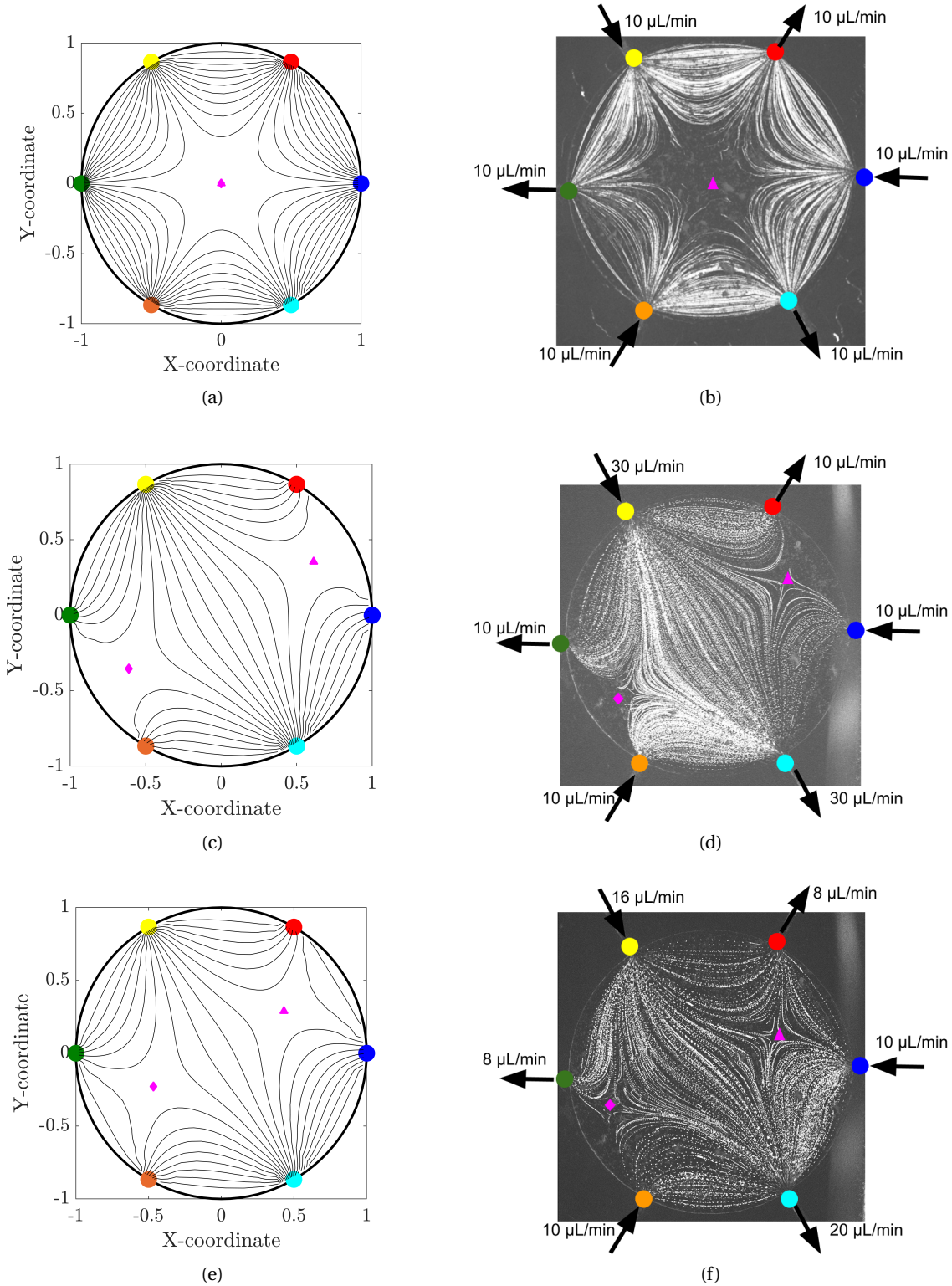

Figure 4.1: Figures (a),(c),(e) shows analytical streamlines and stagnation points and (b), (d) and (f) shows the experimental counterpart

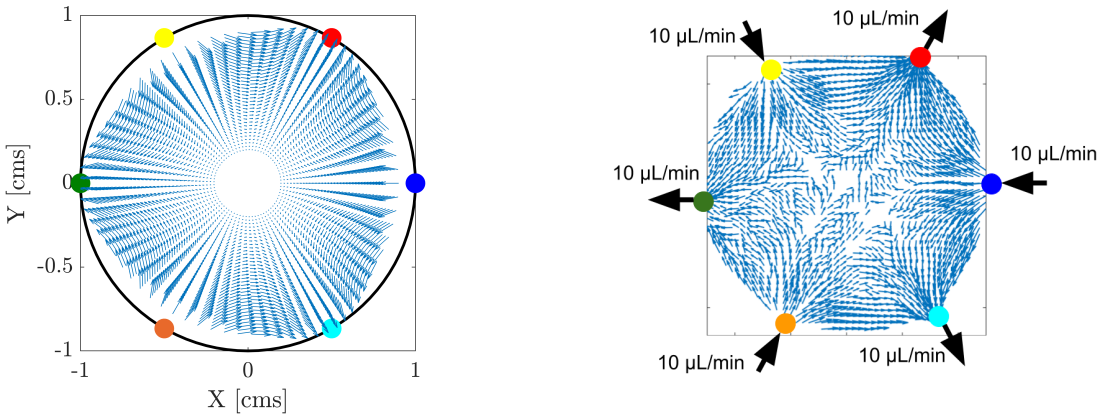

Figure 4.2: Comparison for (a) Analytical and (b) Experimental velocity fields

After comparing the streamline patterns, it was also necessary to look into the velocity fields and quantitatively compare the velocities from analytical and experimental results. These experimental velocity fields were evaluated using Particle Image Velocimetry (PIV). Velocity fields for flow configuration mentioned in figure 4.1b are shown in figure 4.2. The maximum velocity from experiments is approximately 71μm/s and from the analytical solution is around 80μm/s, which shows a good match. In figure, 4.2b there are a few velocity vectors around the centre of the device where there is a stagnation point. The reason for this can be attributed to fluctuations in flow rates which is explicated in more detail in the next section.

Since the device is symmetrical, increasing or decreasing the flow rates should also produce same stagnation point and streamline patterns. The next set of experiments were carried out varying the flow rates keeping the ratio same as mentioned in figure 4.1b.

4.1.1. EFFECT OF VARYING THE FLOW RATES

In this case, the ratio of the flow rates was kept constant and the values were varied. Since, the case chosen is 4.1b, the ratio of the flow rates is 1 and the flow rate values were varied as shown in figures 4.3a, 4.4a, 4.5a and 4.6a. These experiments were done to check the lowest value of flow rates the setup can go upto.

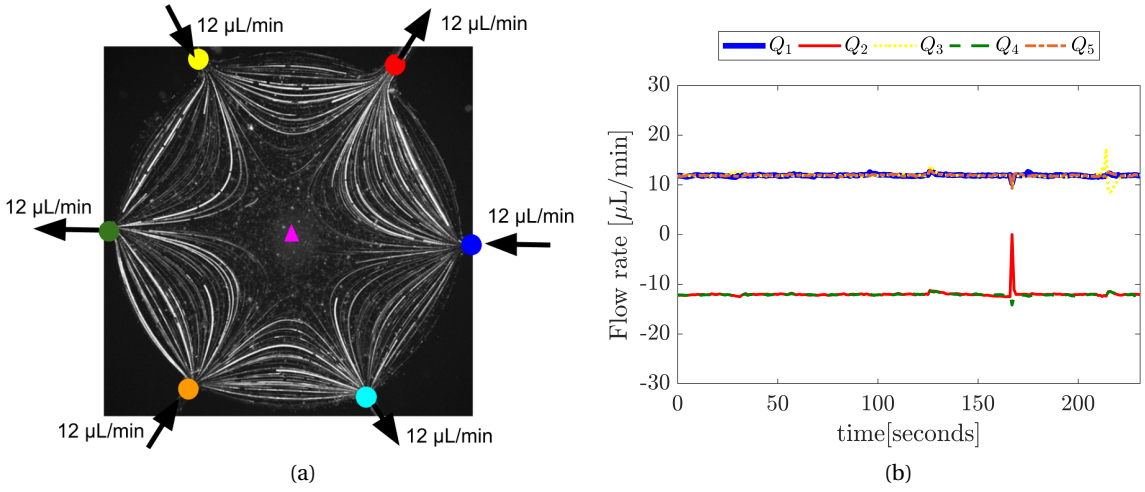

Figure 4.3: (a)Experimental streamlines and (b) flow rate trend from pump as a function of time for Q=12 μL/min

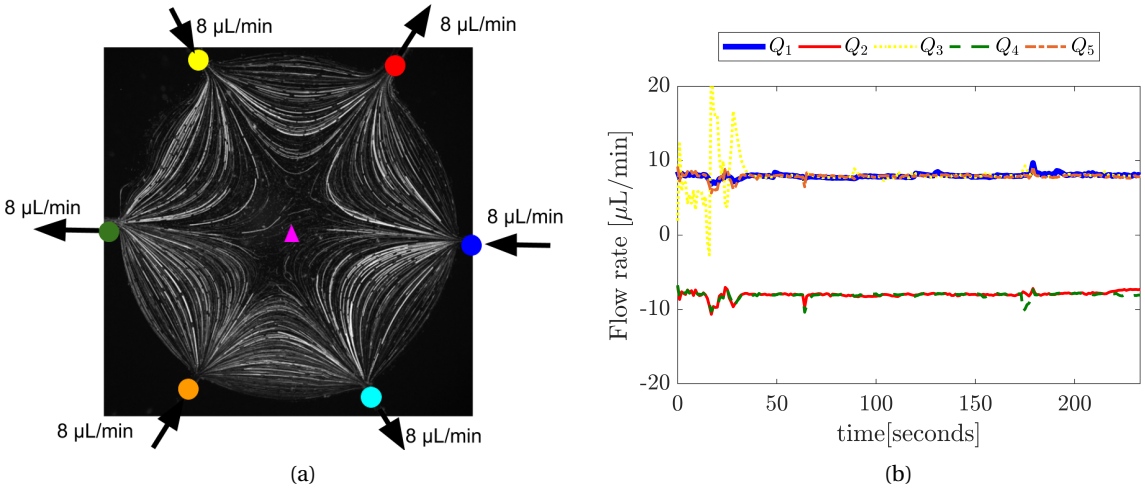

Figure 4.4: (a)Experimental streamlines and (b) flow rate trend from pump as a function of time for Q=8 μL/min

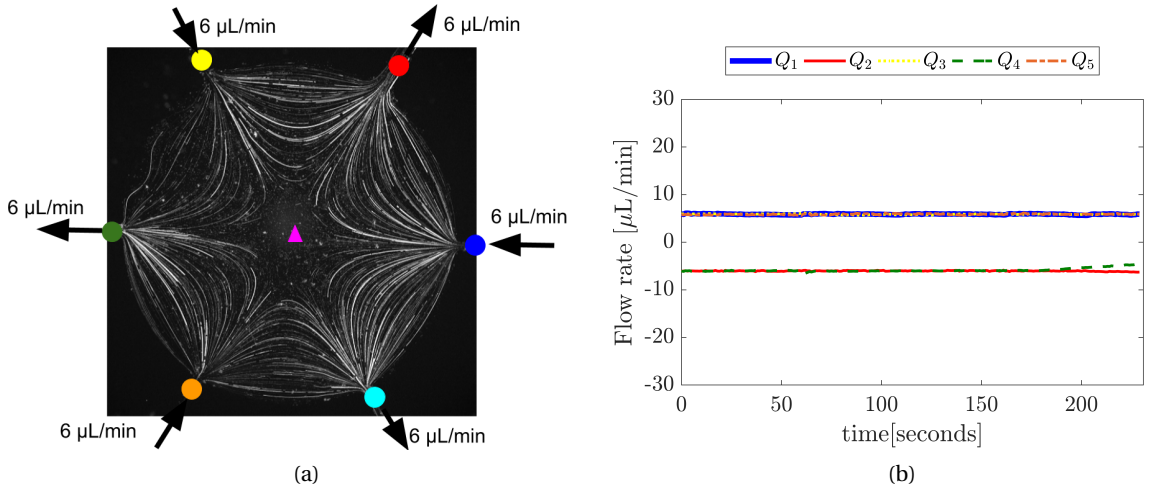

(a) (b)

Figure 4.5: (a)Experimental streamlines and (b) flow rate trend from pump as a function of time for Q=6 μL/min

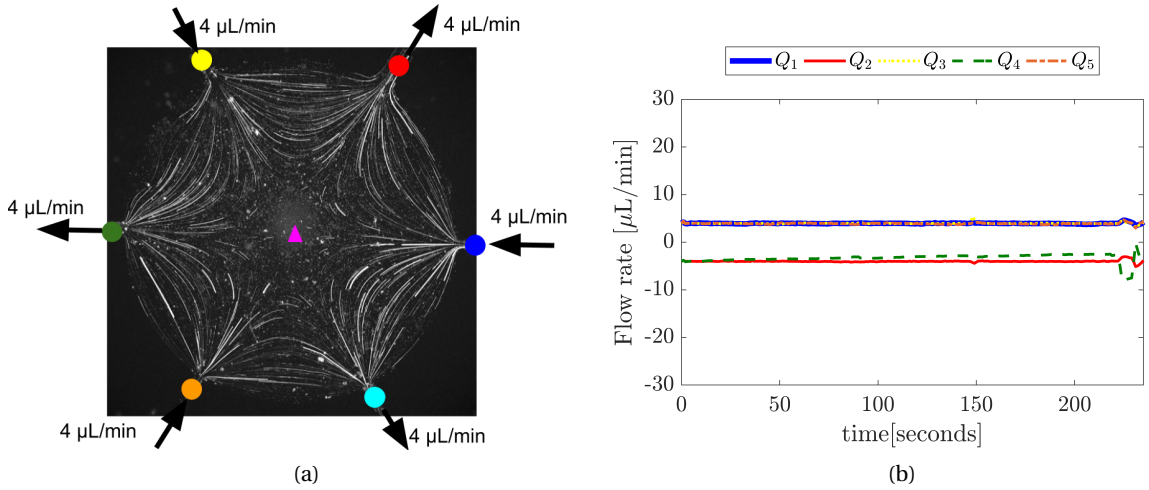

(a) (b)

Figure 4.6: (a) Experimental streamlines and (b) flow rate trend from pump as a function of time for Q=4 μL/min

The minimum flow rate achieved was 4 μL/min as can be seen in figure 4.6a. The lower values of flow rates were attempted and the streamline patterns did not appear clearly due to high fluctuations in flow rates. The reason for fluctuations in flow rates can be attributed either to tracer particles sticking to the tubes in the experimental setup and the microfluidic device or can also be a shortcoming of the pump. To resolve this, experiments were carried out with distilled water to check if the reason for the fluctuations was due to the pressure pump.

The figure 4.7 shows plots of flow rate against time from the pressure pump for the case when DEMI water was used without any tracer particles. The fluctuations in the flow rates even for values as low as 1μL/min are not significantly high. This shows that the fluctuations in flow rates mentioned before are due to tracer particles sticking to the tubings of the experimental setup and is not the problem of the pump.

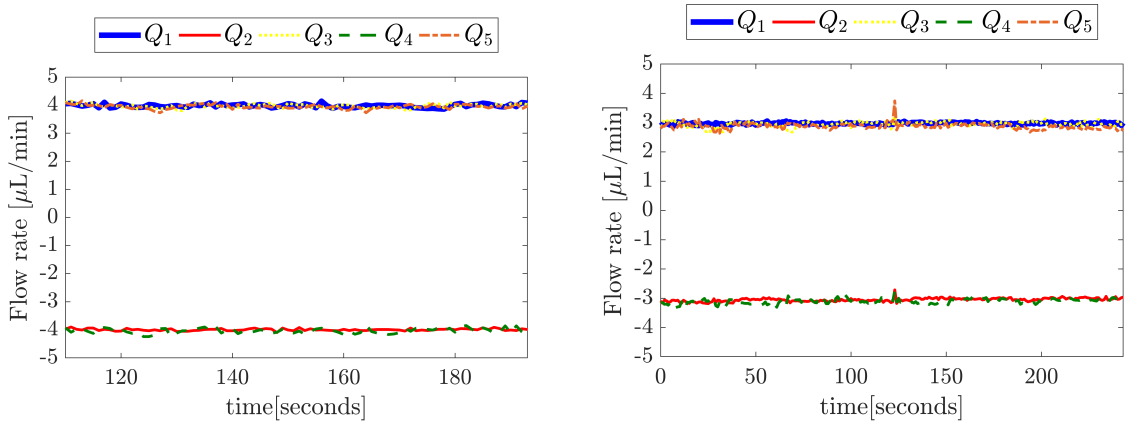

(a) Q=4 μL/min (b) Q=3μL/min

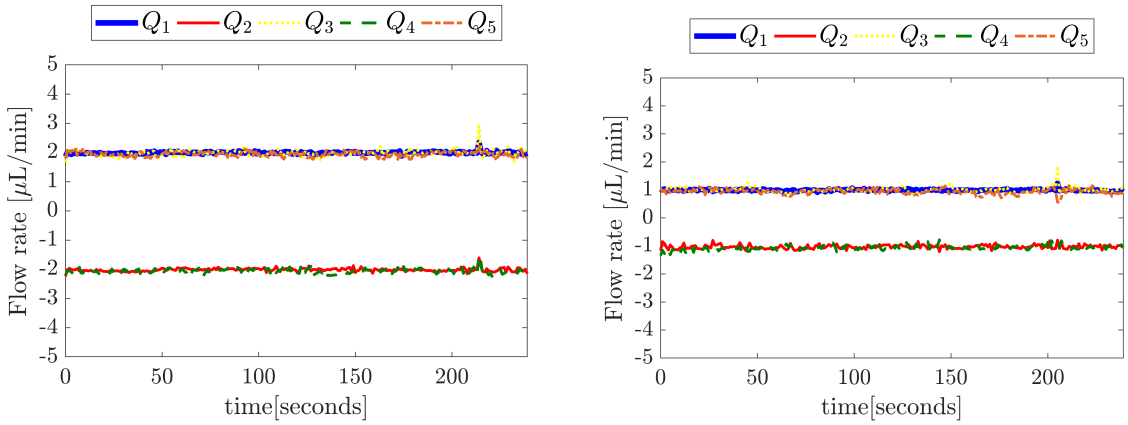

(c) Q=2μL/min (d) Q=1μL/min

Figure 4.7: Flow rate v/s time data from pressure pump for DEMI water with no tracer particles for equal magnitude of flow rates (a) 4μL/min (b) 3μL/min (c) 2μL/min and (d) 1μL/min

5

PARTICLE MANIPULATION USING UNSTEADY FIELDS

Before moving on to manipulating a particle, to check if the flow rates values could be changed with time, movement of stagnation points was checked. The first section described the quasi steady motion of stagnation points and the second section will describe the complex manipulation activities.

5.1. QUASI STEADY MOTION OF STAGNATION POINTS

5.1.1. RANDOM MOTION OF STAGNATION POINTS

The flow rates in two flow ports denoted by Q_3 and Q_6 in figure 3.3 were varied and the movement of stagnation point was checked. This was carried out to check the time the flow rates would take to change once a new value was prescribed.

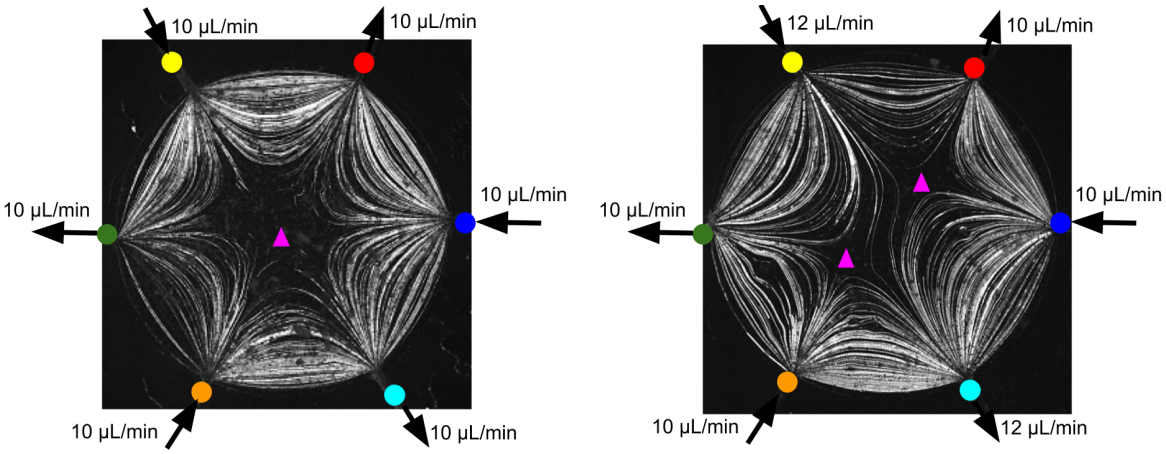

(a) (b)

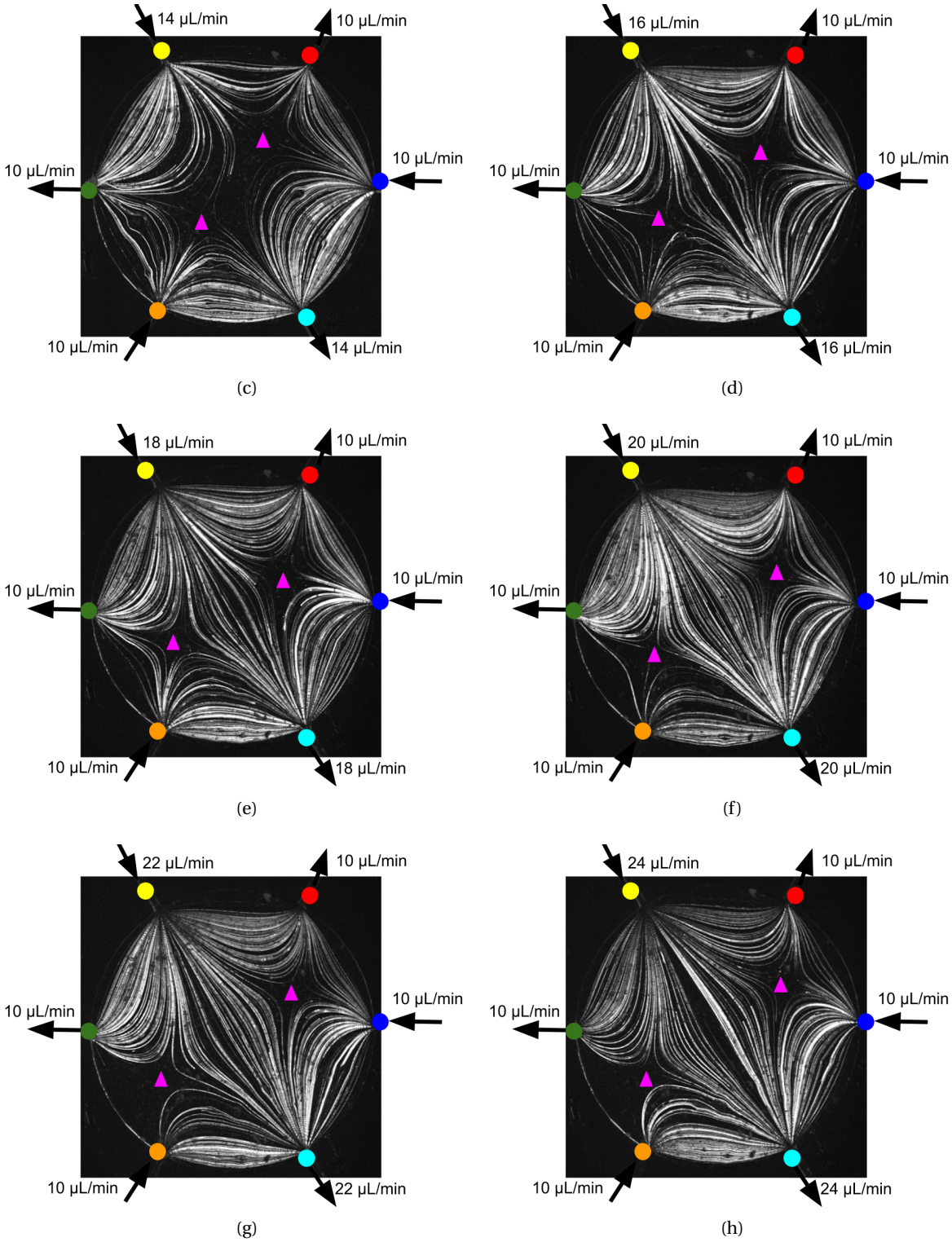

Figure 5.1: Magnitude of flow rates Q_2 and Q_5 varied from (a) 10μL/min to (h)24μL/min with increments of 2μL/min

As can be seen from figures 5.1a to 5.1h the streamline patterns appear clear and the stagnation point split from center in figure 5.1a to two in figure 5.1b. From figures, 5.1bto 5.1h the stagnation point moves randomly. The motion is not shown in the figures since the aim of these experiments was to check if changing the flow rates quasi-steadily gave a clear streamline pattern and movement of the stagnation points.

Since, random motion of stagnation points was achieved movement of stagnation points in a particular shape can also be executed. The next subsection describes the experiments that were conducted to achieve the motion of stagnation points in a circle.

5.1.2. CIRCULAR MOTION OF STAGNATON POINTS

The starting point of this experiment was chosen to be where the stagnation point lied at the center. The flow rates were chosen analytically so that changing them (quasi-steadily) would move the stagnation point in a circle. The analytical results are presented in figures 5.2a, 5.2c, 5.2e, 5.2g and 5.2i the corresponding experimental results and flow configurations are shown in figures 5.2b, 5.2d, 5.2f, 5.2h and 5.2j.

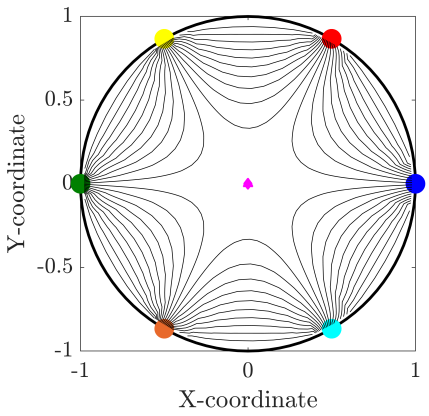

(a)

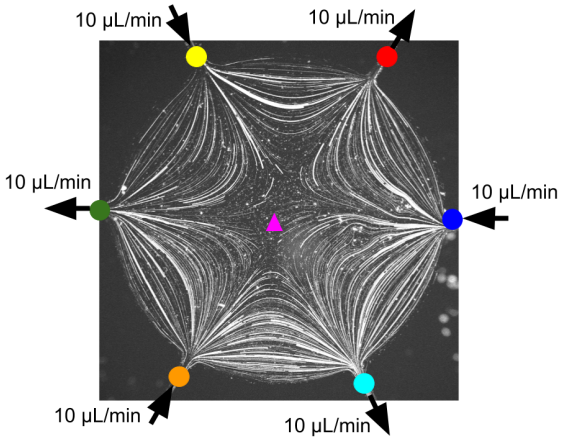

(b)

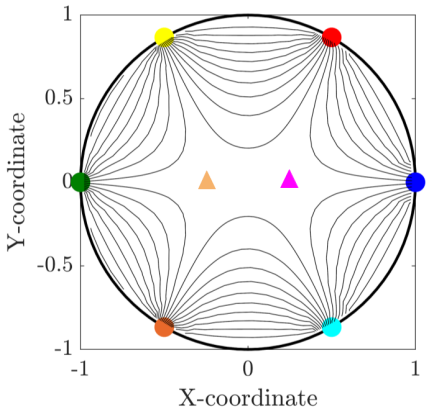

(c)

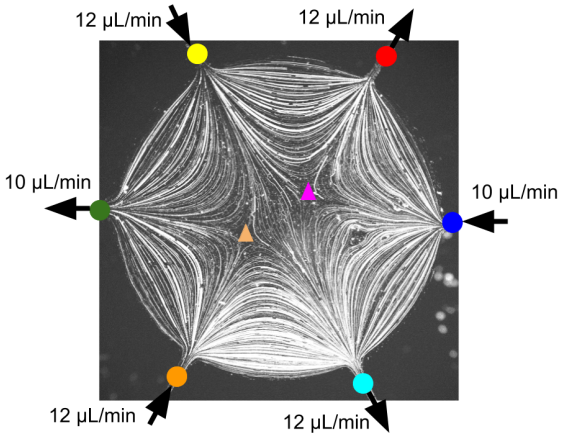

(d)

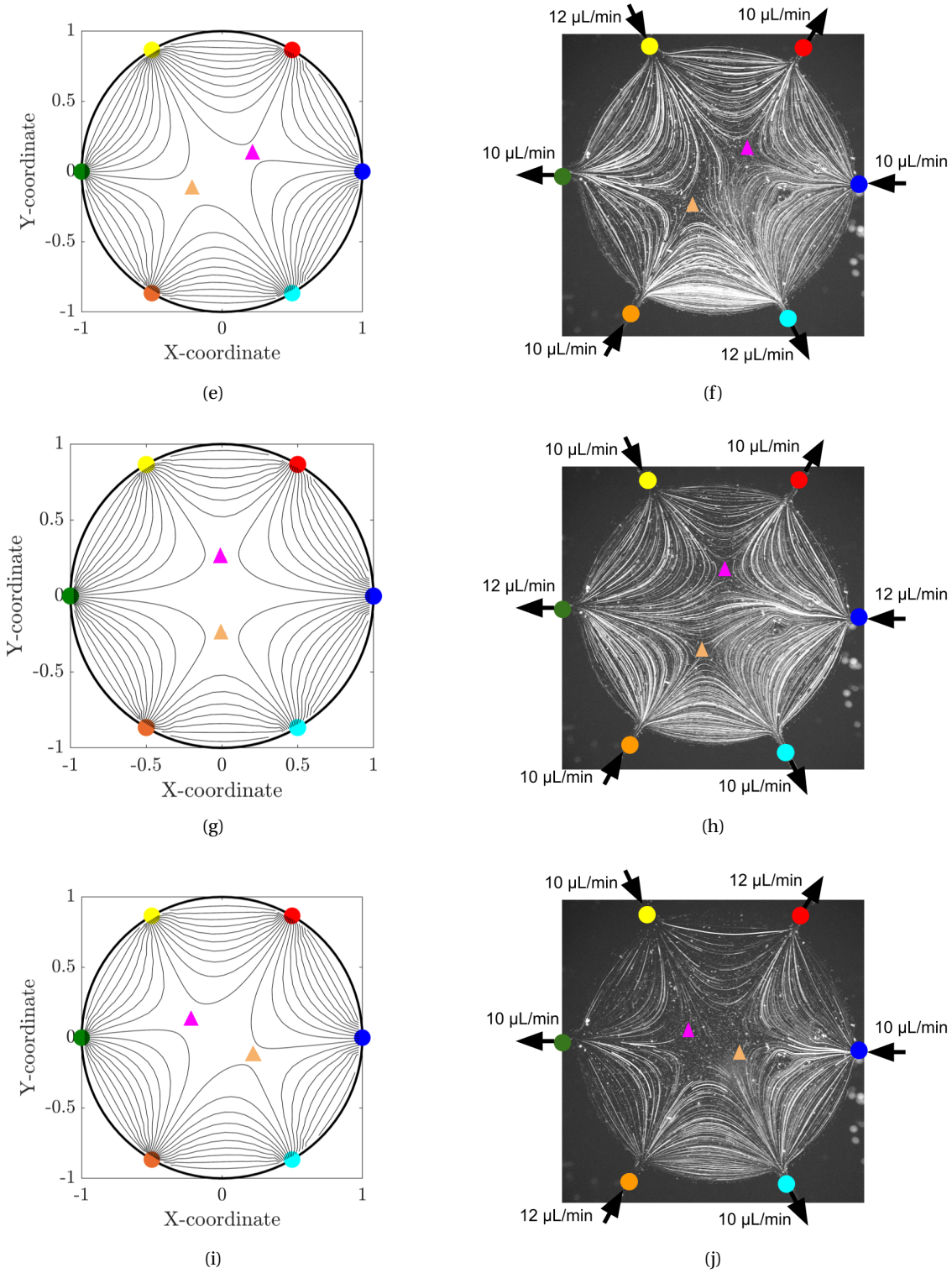

Figure 5.2: Building blocks for movement of stagnation point in a circle

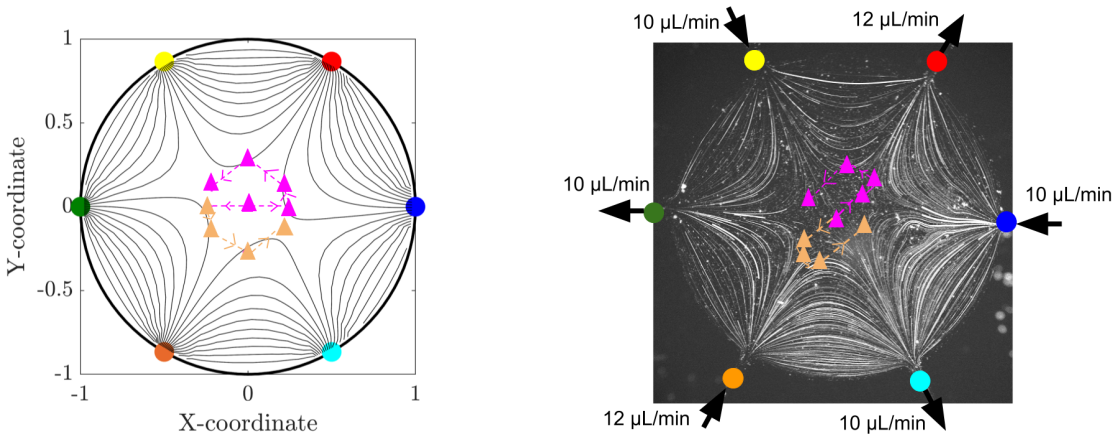

(a) (b)

Figure 5.3: Stagnation point path followed (a) Analytically and (b) Experimentally.

The final results for the movement of stagnation points are shown in figure 5.3a and 5.3b. The experimental manipulation in 5.3b appears to be rotated as compared 5.3a. The reason for this can be found in figures 5.2d and 5.2h when compared to their analytical counterpart. The difference arises since the prescribed flow rate values could not be reached. This is clarified by plotting the flow rate against time to observe the flow ports which could not reach the flow rate values. In figures 5.4a and 5.4b it can be clearly seen that the flow port 2 marked with red could not reach the prescribed value of -12 μL/min and -10 μL/min for the case in figures 5.2d and 5.2h. The negative sign is indicative that it is a sink.

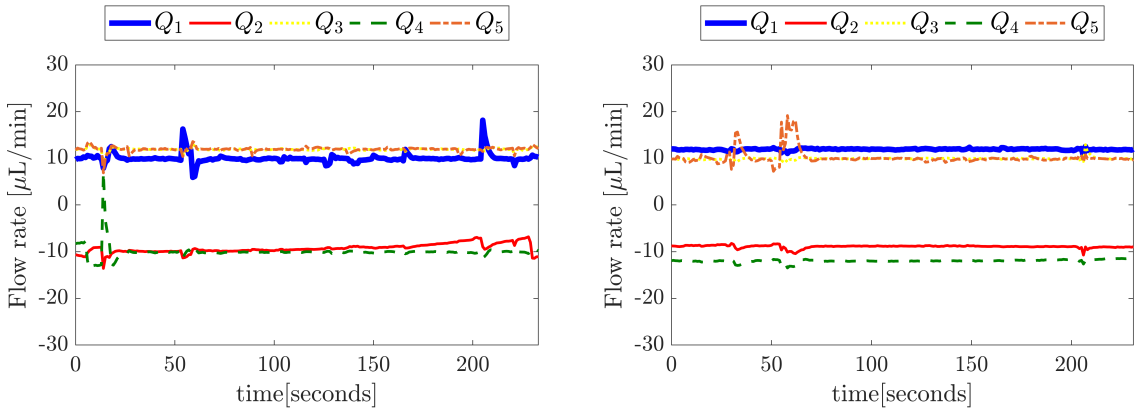

(a) (b)

Figure 5.4: Flow rate v/s time plot from data extracted from the pressure pump for (a)figure 5.2d and (b) figure 5.2h

To check whether the experimental results in figures 5.2d and 5.2h match with analytical counterpart, the flow rates achieved by the pump in figures 5.4a and 5.4b can be used an input for the analytical solution. The figure 5.4 along with figure 5.5 give a complete closure to the deviation of circular motion of stagnation point in figure 5.3b from figure 5.3a.

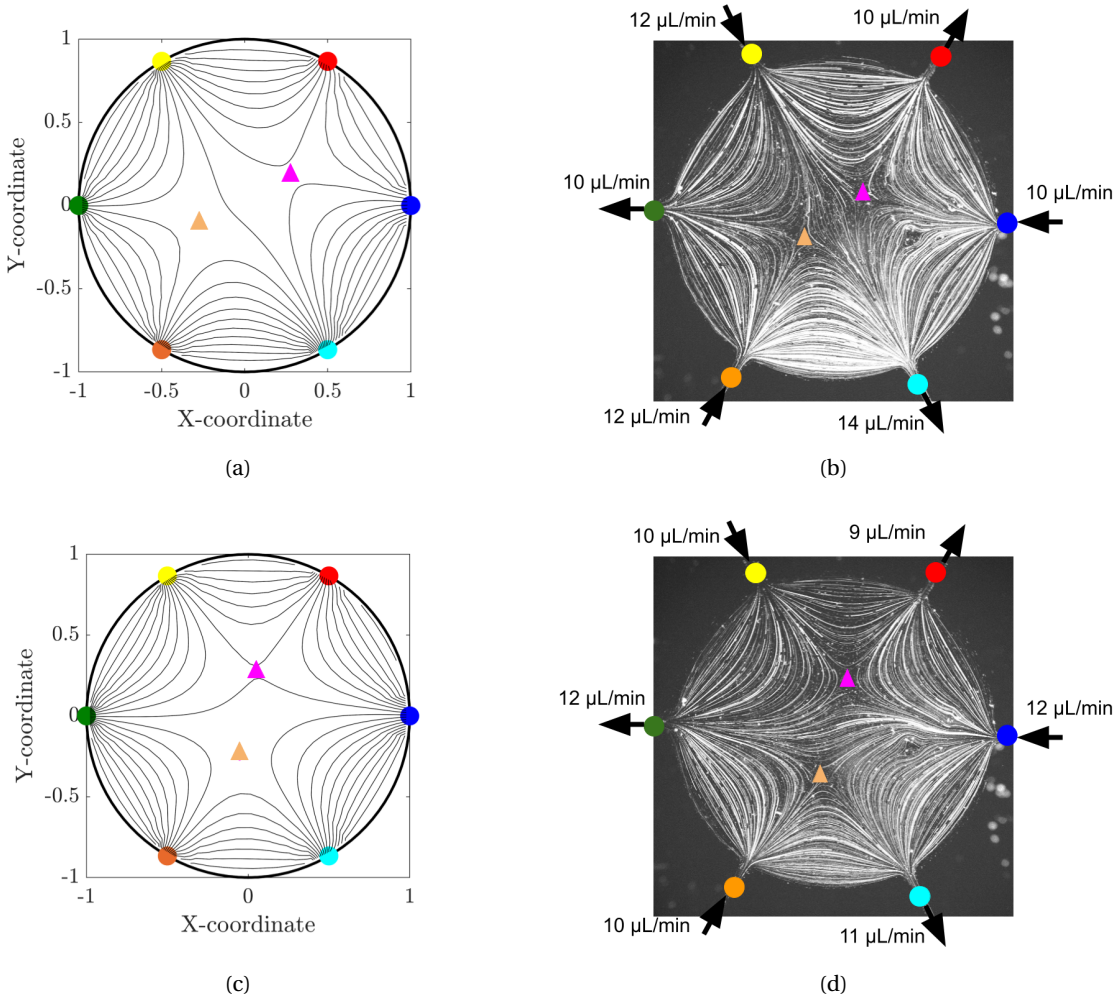

Figure 5.5: Comparison for (a),(c) analytical and experimental (b),(d) streamlines and stagnation point for from flow rates values in figures 5.4a and 5.4b

As it can be observed from figures 5.4a and 5.4b, the flow port 2 which is a sink could not reach the prescribed flow rate. However, if a certain back pressure value is given in flow port 6 then flow rates can be reached in all the sources and sinks.

5.2. SINGLE PARTICLE MANIPULATION

A single particle of diameter 150-180 μm with density 1.001 g/cc was introduced in the device. The particle was surface treated in the same way as the tracer particles were surface treated as mentioned in chapter 4. After the particle entered the device, various manipulation activities were carried out. Firstly the particle was trapped at the center of the device for sometime. Also, various manipulation activities were carried out using the streamlines of various flow configurations

5.2.1. PARTICLE TRAPPING

Before moving to the particle manipulation, the flow ports are colour coded similar to the ones used in the section 5.1. As the particle was introduced in the device, it was captured at a position highlighted in figure 5.6a at time t=0. The idea was to the bring the particle to the center of the device. The flow configuration of the ports was adjusted so that the particle followed the path through figures 5.6b, 5.6c to 5.6d and the time mentioned is the time at which it reached the respective position.

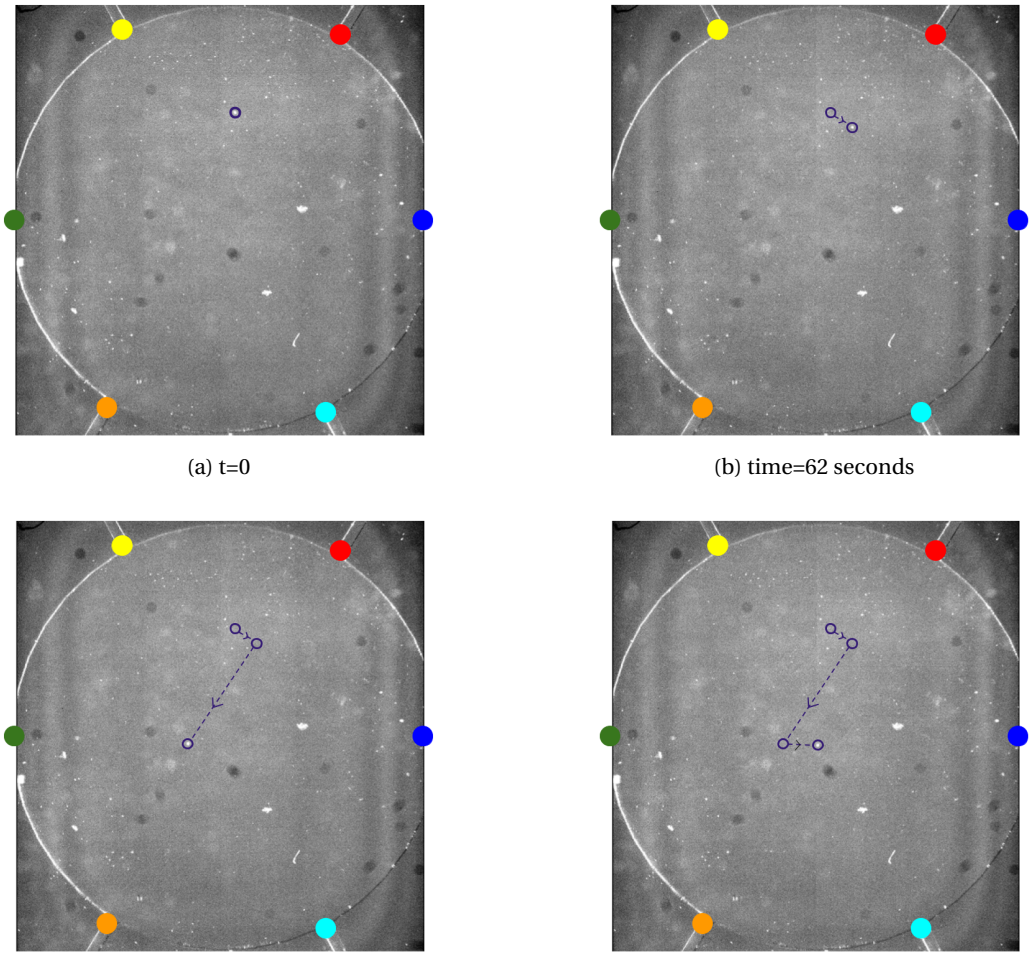

(a) t=0

(b) time=62 seconds

(c) time = 140 seconds

(d) time = 208 seconds

Figure 5.6: Particle entered, stopped at position in (a) and followed the path as shown in (b), (c) and (d) respectively

Since the position of the particle is at the center of the device, the flow ports were configured to the flow rates shown in figure 5.7. According to the figure 4.1b, the stagnation point for the flow

configuration in figure 5.7 lies at the center of the device. Therefore, the particle is trapped at the center. However, the particle was trapped at the center for a time of approximately 131 seconds (≈ 2 minutes).

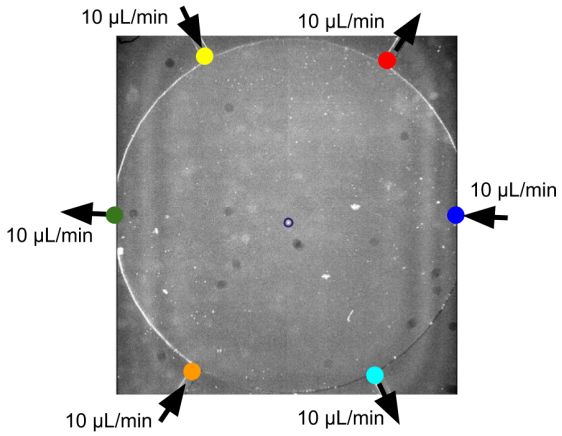

Figure 5.7: Flow port configuration with particle at the centre

5.2.2. MANIPULATING SINGLE PARTICLE

Single particle manipulation activities consisting of tracing English alphabets were carried out. A few of these manipulations are explained here. Multiple letters could be traced using a single particle using the flow rates from the sources and sinks. In a few cases, the particle did not move along the desired pathline so the particles could not be traced perfectly.

To begin with, the particle entered through flow port 2 (refer figure 3.3). Since the manipulation is done manually the position where the particle would stop cannot be controlled. This is the reason why a few alphabets might appear rotated but for clarity the device is adjusted so that the final form of the letters appear clearly. The first English alphabet that was traced was the letter N and is clearly shown in figure 5.8. The particle was first trapped at the location shown in figure 5.8a and this time was t=0. The first stem of N, was made as shown in figure 5.8b and the time mentioned in the sub-caption represents the time at which the particle reached the highlighted location with arrow pointing towards the position. The flow ports were configured such that the alphabet could be traced as shown in figure 5.8.

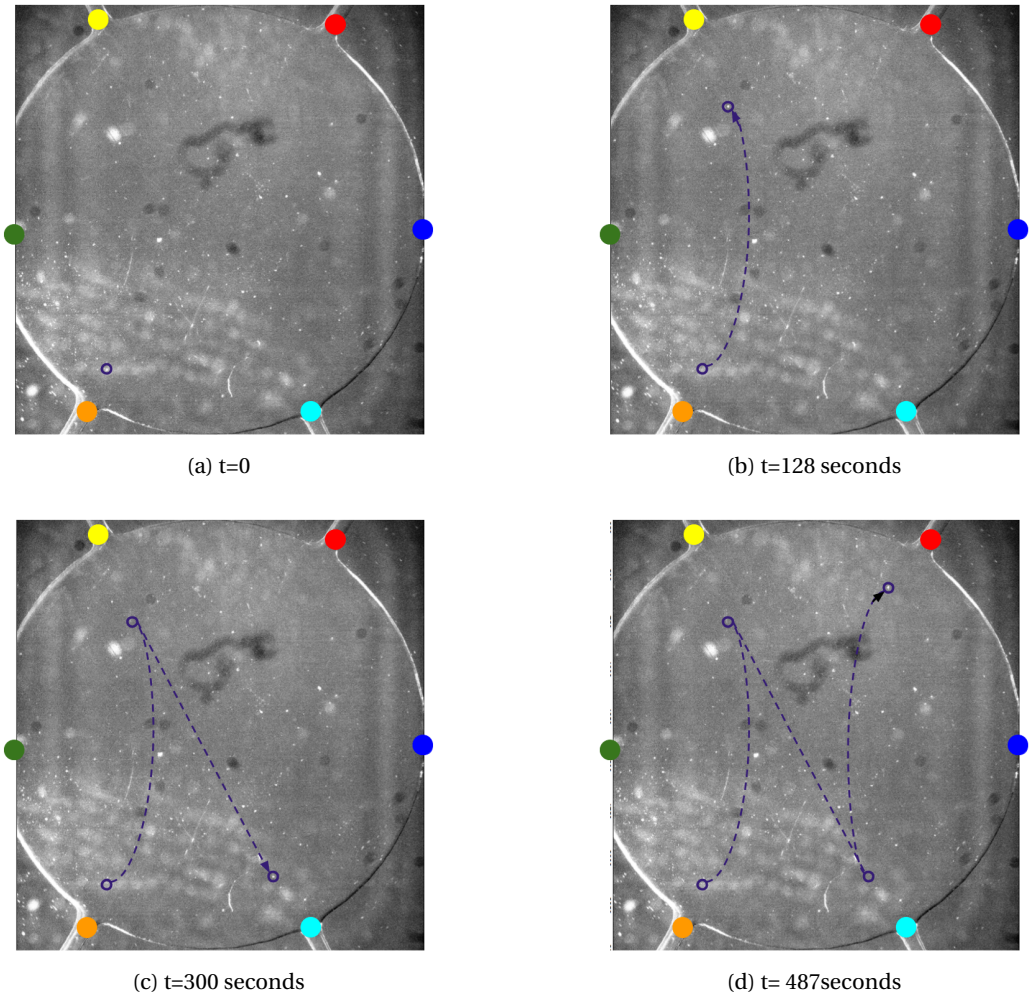

(a) t=0

(b) t=128 seconds

(c) t=300 seconds

(d) t= 487seconds

Figure 5.8: Single particle manipulation to form a letter N

In figure 5.8 only one letter could be traced using a single particle, However, there are multiple alphabets which can be traced by a single particle in continuous manner. One such case is mentioned

in figure 5.9 where the letter T,J and I are formed in succession using the same single particle. This could be carried out because of the similar structure of the mentioned alphabets. The particle was first trapped at the location shown in figure 5.9a. Furthermore, the flow ports were controlled such that the pathline followed by the particle traced the letters as shown in figures 5.9e, 5.9f and 5.9g.

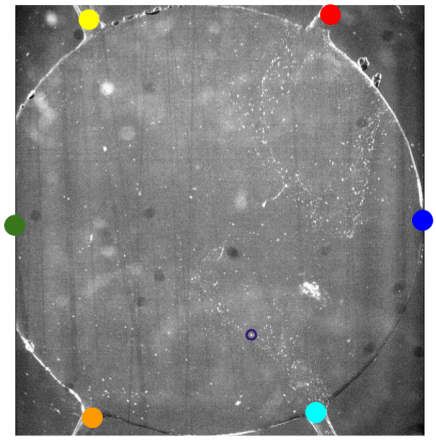

(a) t=0

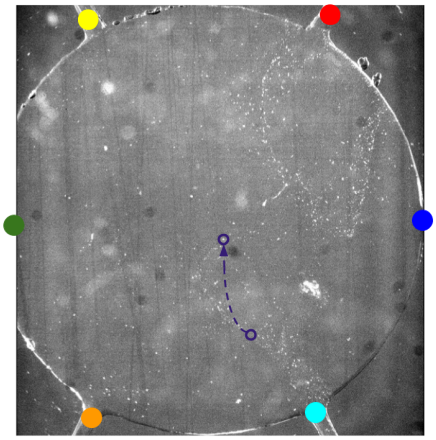

(b) t=295 seconds

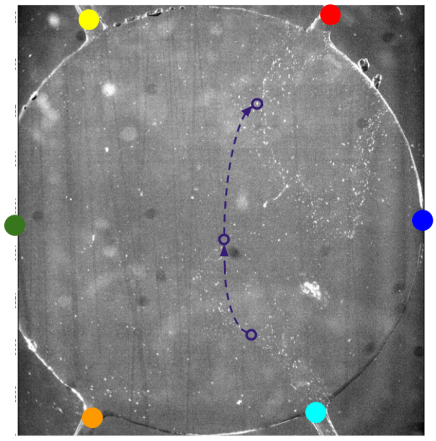

(c) t=420 seconds

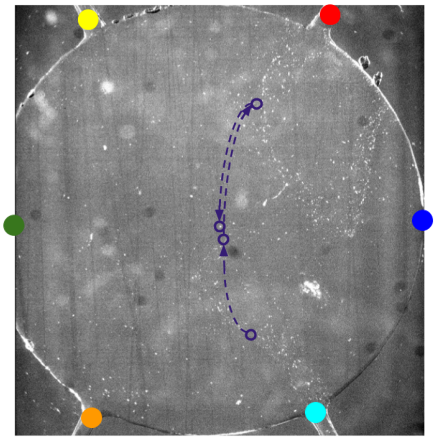

(d) t=532 seconds

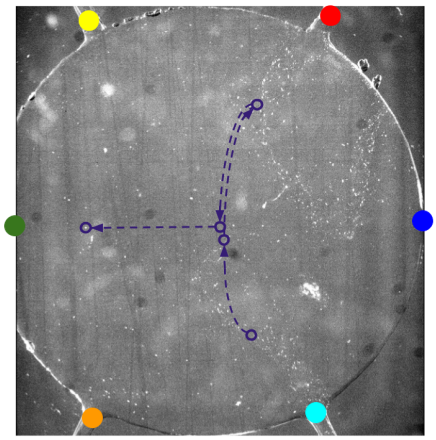

(e) t=640 seconds

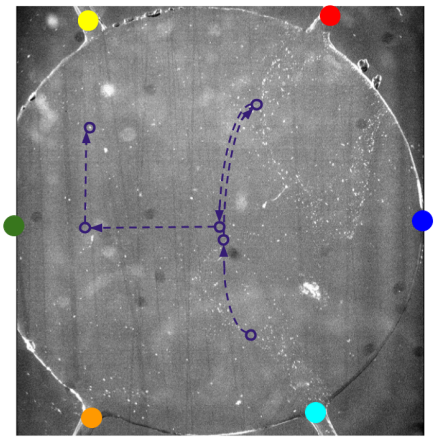

(f) t = 765 seconds

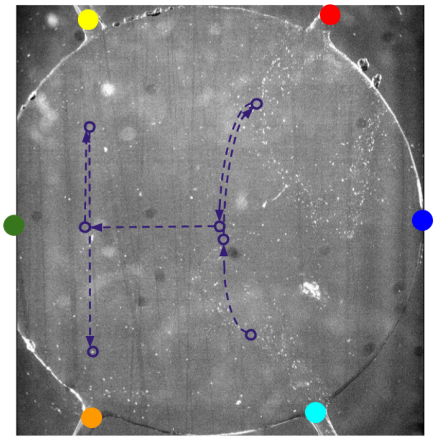

(g) t=880 seconds

Figure 5.9: Particle used to form multiple alphabets(T,J,I) in one go

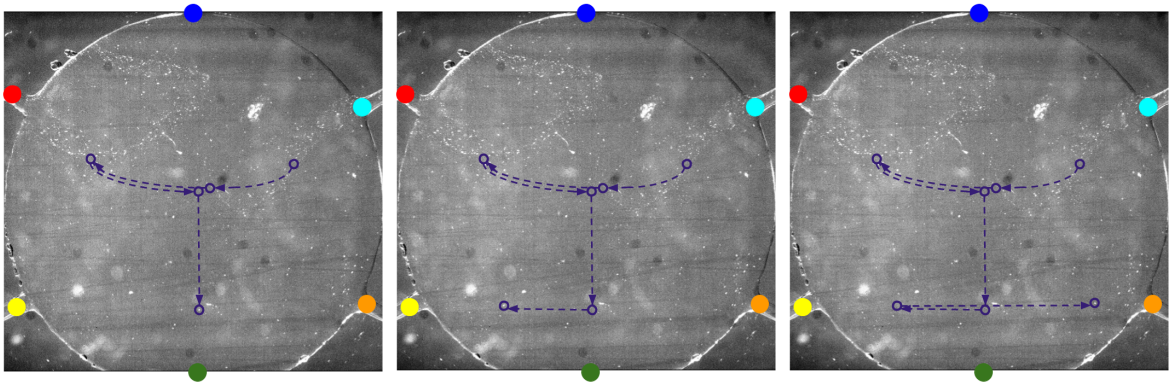

(a) Letter T (b) Letter J (c) Letter I

Figure 5.10: Device rotated by an angle of 90 degree counter-clockwise to observe the letters better

For clarity, the device is rotated by an angle of 90 degree counter-clockwise for better readability of the alphabets as shown in figure 5.10. The first English alphabet 'A' was also traced using a single particle as shown in figure 5.11. The particle followed the pathline as shown in figures 5.11a,5.11b,5.11c,5.11d and 5.11e to make the alphabet A. Again, to clearly see the letter the device is rotated as shown in figure 5.12.

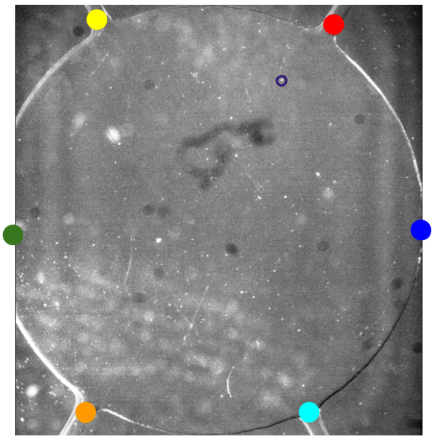

(a) t=0

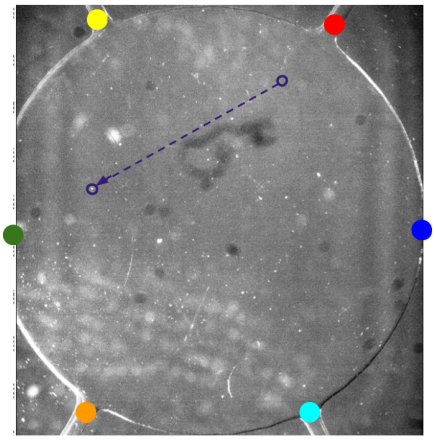

(b) t=116 seconds

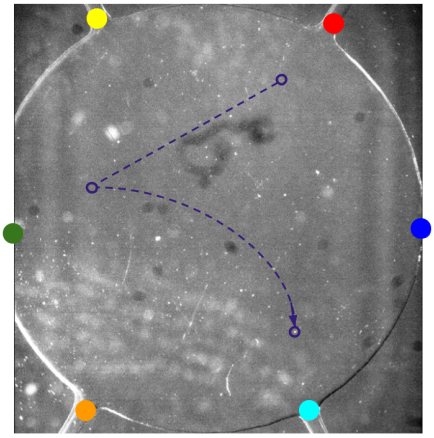

(c) t=376 seconds

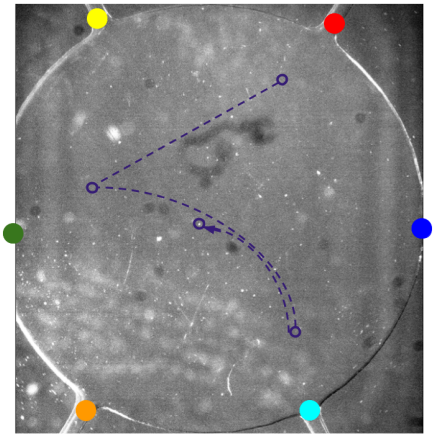

(d) t=613 seconds

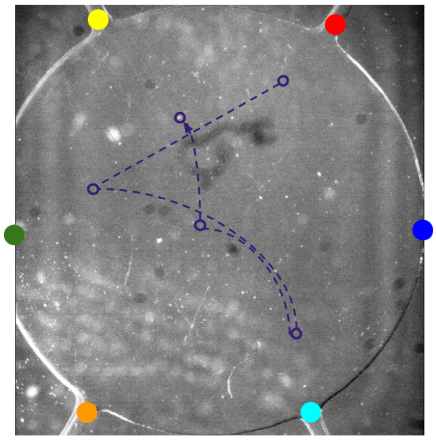

(e) t=830 seconds

Figure 5.11: Forming the English letter A

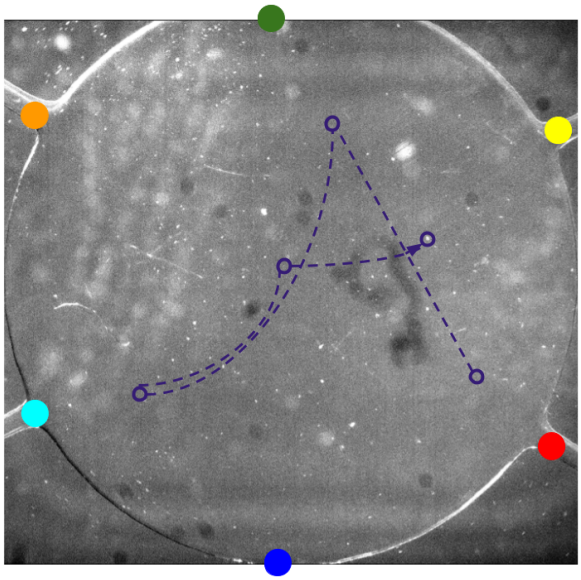

Figure 5.12: Device rotated by 90 degree clockwise for letter A

The manipulation activities for tracing alphabets are not limited to the ones mentioned here. There were more alphabets that were traced successfully and are mentioned in the appendix B.

6

CONCLUSIONS AND RECOMMENDATIONS

The focus of the thesis was to design and fabricate a microfluidic device to manipulate two particles simultaneously. The first step would be to design the device and validate it before manipulating particles.

The device was designed such that it was a Hele-Shaw flow cell. The potential flow in the circular chamber was solved analytically. The device was fabricated after 3D printing the mould using PDMS as the polymer. Experiments were conducted using volume illuminated PIV for different flow configurations. The device was then validated by comparing experimental streamlines and stagnation points to analytical solution for different flow configuration.

Particle manipulation requires the flow rates to be changed with time to generate unsteady flow field. To achieve that flow rates were first varied quasi steadily to check the movement of stagnation points. Stagnation points were moved in a circular fashion. However, the experimental results deviated from the analytical results. The reason for that was the tracer particles sticking in the tubings of the experimental setup and the PDMS device, resulting in fluctuations in the flow rates.

Finally, a particle was introduced in the device and manipulation activities were carried out. Firstly, the particle was trapped at the centre for a limited time. Additionally, complex manipulation activities were carried out using a single particle. This manipulation activity was carried out by manually controlling the flow rates and moving the particle along a streamline.

Control algorithms have been established in literature to manipulate two particles using two stagnation points. Since, two stagnation points can be generated in the current device two particles can also be manipulated. Until now, manipulation activities were executed using single particle. The novelty of this approach is that the streamlines were used to manipulate a single particle. Based on this, it should be possible to manipulate two particles along streamlines.

6.1. RECOMMENDATIONS

Firstly manipulation of a single particle should be carried with tracer particles to generate vector plots and streamlines. It would then be possible to represent particle moving along a streamline. Furthermore, single particle manipulation should be carried out using a control loop including the pump and camera to gain better control over the particle. This will ensure the pathline that the particle will follow, thereby giving perfect English alphabets.

Furthermore, manipulating two particles by making a optimization algorithm as mentioned in appendix C should also be carried out. The first step in this algorithm should be to get the location of the particles as they enter the device. This location will be the input to the pump such that the trajectory of the particles can be decided based on the final locations of the particle.

Literature has stated that only two particles can be manipulated using the kind of device used in thesis. However, in literature stagnation points have been used to manipulate the particles. The novelty of this technique lies in the use of streamlines to manipulate particles, so it might also be possible to manipulate two or more particles using the same device design.

BIBLIOGRAPHY

[1] G. I. Taylor, *The Formation of Emulsions in Definable Fields of Flow,* Proceedings of the Royal Society A: Mathematical, Physical and Engineering Sciences **146**, 501 (2006), arXiv:0511310 [arXiv:cond-mat] .

[2] B. J. Bentley and L. G. Leal, *A computer-controlled four-roll mill for investigations of particle and drop dynamics in two-dimensional linear shear flows,* Journal of Fluid Mechanics Digital Archive **167**, 219 (2006).

[3] M. Tanyeri, E. M. Johnson-Chavarria, and C. M. Schroeder, *Hydrodynamic trap for single particles and cells,* Applied Physics Letters **96** (2010), 10.1063/1.3431664.

[4] A. Shenoy, C. V. Rao, and C. M. Schroeder, *Stokes trap for multiplexed particle manipulation and assembly using fluidics,* Proceedings of the National Academy of Sciences **113**, 3976 (2016).

[5] J. T. Kuo, L. Yu, and E. Meng, *Micromachined thermal flow sensors-A review,* Micromachines **3**, 550 (2012).

[6] L. Mazutis and A. D. Griffiths, *Selective droplet coalescence using microfluidic systems,* Lab on a Chip **12**, 1800 (2012).

[7] Y. C. Tan, Y. L. Ho, and A. P. Lee, *Droplet coalescence by geometrically mediated flow in microfluidic channels,* Microfluidics and Nanofluidics **3**, 495 (2007).

[8] D. R. Link, E. Grasland-Mongrain, A. Duri, F. Sarrazin, Z. Cheng, G. Cristobal, M. Marquez, and D. A. Weitz, *Electric control of droplets in microfluidic devices,* Angewandte Chemie - International Edition **45**, 2556 (2006).

[9] M. H. Schneider, V. J. Sieben, A. M. Kharrat, and F. Mostowfi, *Measurement of asphaltenes using optical spectroscopy on a microfluidic platform,* Analytical Chemistry **85**, 5153 (2013).

[10] R. Fisher, M. K. Shah, D. Eskin, K. Schmidt, A. Singh, S. Molla, and F. Mostowfi, *Equilibrium gas-oil ratio measurements using a microfluidic technique,* Lab on a Chip **13**, 2623 (2013).

[11] K. Hoshino, Y. Y. Huang, N. Lane, M. Huebschman, J. W. Uhr, E. P. Frenkel, and X. Zhang, *Microchip-based immunomagnetic detection of circulating tumor cells,* Lab on a Chip **11**, 3449 (2011).

[12] H. W. Hou, M. E. Warkiani, B. L. Khoo, Z. R. Li, R. A. Soo, D. S. W. Tan, W. T. Lim, J. Han, A. A. S. Bhagat, and C. T. Lim, *Isolation and retrieval of circulating tumor cells using centrifugal forces,* Scientific Reports **3**, 1 (2013).

[13] J. H. Kang, S. Krause, H. Tobin, A. Mammoto, M. Kanapathipillai, and D. E. Ingber, *A combined micromagnetic-microfluidic device for rapid capture and culture of rare circulating tumor cells,* Lab on a Chip **12**, 2175 (2012).

[14] A. R. Wheeler, W. R. Throndset, R. J. Whelan, A. M. Leach, R. N. Zare, Y. H. Liao, K. Farrell, I. D. Manger, and A. Daridon, *Microfluidic device for single-cell analysis,* Analytical Chemistry **75**, 3581 (2003).

[15] E. Brouzes, M. Medkova, N. Savenelli, D. Marran, M. Twardowski, J. B. Hutchison, J. M. Rothberg, D. R. Link, N. Perrimon, and M. L. Samuels, *Cytotoxicity Screen,* Proceedings of the National Academy of Sciences of the United States of America **106**, 14195 (2009).

[16] D. Dendukuri and P. S. Doyle, *The synthesis and assembly of polymeric microparticles using microfluidics,* Advanced Materials **21**, 4071 (2009).

[17] D. Philp and J. Fraser Stoddart, *Self-Assembly in natural and unnatural systems,* Angewandte Chemie (International Edition in English) **35**, 1154 (1996).

[18] G. M. Whitesides and B. Grzybowski, *Self-assembly at all scales,* Science **295**, 2418 (2002).

[19] X. Hu, P. H. Bessette, J. Qian, C. D. Meinhart, P. S. Daugherty, and H. T. Soh, *Marker-specific sorting of rare cells using dielectrophoresis,* Proceedings of the National Academy of Sciences **102**, 15757 (2005).

[20] J. R. Moffitt, Y. R. Chemla, S. B. Smith, and C. Bustamante, *Recent Advances in Optical Tweezers,* Annual Review of Biochemistry **77**, 205 (2008).

[21] Z. Liu, F. Huang, J. Du, W. Shu, H. Feng, X. Xu, and Y. Chen, *Rapid isolation of cancer cells using microfluidic deterministic lateral displacement structure,* Biomicrofluidics **7** (2013), 10.1063/1.4774308.

[22] J. Takagi, M. Yamada, M. Yasuda, and M. Seki, *Continuous particle separation in a microchannel having asymmetrically arranged multiple branches,* Lab on a Chip **5**, 778 (2005).

[23] M. Tanyeri, M. Ranka, N. Sittipolkul, and C. M. Schroeder, *A microfluidic-based hydrodynamic trap: Design and implementation,* Lab on a Chip **11**, 1786 (2011).

[24] D. D. Carlo, L. Y. Wu, and L. P. Lee, *Dynamic single cell culture array,* Lab on a Chip **6**, 1445 (2006).

[25] A. Shenoy, M. Tanyeri, and C. M. Schroeder, *Characterizing the performance of the hydrodynamic trap using a control-based approach,* Microfluidics and Nanofluidics (2015), 10.1007/s10404-014-1495-7.

[26] T. M. Schneider, S. Mandre, and M. P. Brenner, *Algorithm for a microfluidic assembly line,* Physical Review Letters **106**, 1 (2011).

[27] J. Happel and H. Brenner, *Low Reynolds number Hydrodynamics: with special applications to particulate media* (2012).

[28] L. Jolla, *The motion of particles in the Hele-Shaw cell,* **261**, 199 (1994).

[29] A. K. Deka, *Manipulation of particles in a Hele-Shaw cell using sources and sinks,* Ph.D. thesis.

[30] E. DM and S. EK, *Positioning single atoms with scanning tunnelling microscope,* Nature **344**, 524 (1990).

[31] M. Hashimoto, P. Garstecki, H. A. Stone, and G. M. Whitesides, *Interfacial instabilities in a microfluidic Hele-Shaw cell,* Soft Matter **4**, 1403 (2008).

[32] Y. Xia and G. M. Whitesides, *SOFT LITHOGRAPHY,* Annual Review of Materials Science **28**, 153 (1998).

[33] G. M. Whitesides, *The origins and the future of microfluidics,* **442** (2006), 10.1038/nature05058.

[34] S.-y. Teh, R. Lin, L.-h. Hung, and A. P. Lee, *Droplet microfluidics,* , 198 (2008).

[35] L. Mazutis and A. D. Griffiths, *Preparation of monodisperse emulsions by hydrodynamic size fractionation,* Applied Physics Letters **95**, 1 (2009).

[36] P. K. Kundu, I. M. Cohen, and D. R. Dowling, *Fluid Mechanics* (2016).

[37] D. Kumar, *A Microfluidic Device for Producing Controlled Collisions Between Two Soft Particles,* (2016).

[38] B. J. Kirby, *Micro and Nanoscale Fluid Mechanics. Transport in Microfluidic Devices* (2010).

[39] R. J. Adrian and J. Westerweel, *Particle Image Velocimetry* (2011).

A

APPENDIX A

As can be seen from the figure(put the flow device design here), we have one equation for mass conservation:

$$\sum_{i=1}^{6} Q_i = 0 \tag{A.1}$$

Using the fact that the height averaged velocity in a Hele-Shaw flow is irrotational as proven earlier, equation A.2 is the condition of irrotationality in polar coordinates.

$$\frac{\partial^2 \psi}{\partial r^2} + \frac{1}{r}\frac{\partial \psi}{\partial r} + \frac{1}{r}\frac{\partial^2 \psi}{\partial \theta} = 0 \tag{A.2}$$

Equation A.3 is the boundary condition for a device with radius r_0.

$$\psi|_{r=r_0} = \sum_{i=1}^{6} Q_i H(\theta - \frac{(i-1)*\pi}{3}) \tag{A.3}$$

where, H represents Heaviside function

$$H(x) = \begin{cases} 1 & \text{if } x > 1 \\ 0.5 & \text{if } x = 0 \\ 0 & \text{if } x < 0 \end{cases} \tag{A.4}$$

A general solution can be written for equation A.2 can be written as:

$$\boxed{\psi = A_0 + \sum_{n=1}^{\infty} r^n [A_n \cos(n\theta) + B_n \sin(n\theta)]} \tag{A.5}$$

where, n are the number of eigenmodes required to converge to the exact solution.

$$\psi|_{r=r_0} = A_0 + \sum_{n=1}^{\infty} r_0^n [A_n \cos(n\theta) + B_n \sin(n\theta)] = \sum_{m=1}^{6} Q_i H(\theta - \frac{(i-1)*\pi}{3})$$

$$\boxed{A_0 + \sum_{n=1}^{\infty} r_0^n [A_n \cos(n\theta) + B_n \sin(n\theta)] = \sum_{m=1}^{6} Q_i H(\theta - \frac{(i-1)*\pi}{3})} \tag{A.6}$$

The coefficients A_0, A_n and B_n can be calculated by using the orthogonality condition along with the boundary condition.

Integrating with respect to θ with limits from 0 to 2π, we get A_0

$$
\begin{aligned}
A_0 &= \frac{1}{2\pi}\int_0^{2\pi}\sum_{i=1}^{6} Q_i H[\theta - \frac{(i-1)\pi}{3}]d\theta \\
&= \frac{1}{2\pi}\sum_{i=1}^{6} Q_m \int_0^{2\pi} H[\theta - \frac{(i-1)\pi}{3}]d\theta \\
&= \frac{1}{2\pi}\sum_{i=1}^{6} Q_m (2\pi - \frac{(i-1)\pi}{3}) \\
&= \frac{1}{2}\sum_{i=1}^{6} Q_i (7-i) \\
&= \frac{1}{6}[\sum_{i=1}^{5} Q_i (7-i) + Q_6 && \text{(separating } Q_6 \text{ from the summation)} \\
&= \frac{1}{6}[\sum_{i=1}^{5} Q_i (7-i) - \sum_{i=1}^{5} Q_m] && \text{(Using equation A.1)} \\
&= \frac{1}{6}\sum_{i=1}^{5} Q_i (6-i)
\end{aligned}
$$

$$
\boxed{A_0 = \frac{1}{6}\sum_{i=1}^{5} Q_i (6-i)} \tag{A.8}
$$

Multiply the equation by A.6 by $\cos(n\theta)$, integrate with respect to θ from 0 to 2π and using the orthogonality condition we get the value for A_n

$$
\begin{aligned}
A_n \int_0^{2\pi} r_0^n \cos^2(n\theta)d\theta &= \int_0^{2\pi}\sum_{i=1}^{6} Q_i H\Big[\theta - \frac{(i-1)\pi}{3}\Big]\cos(n\theta)d\theta \\
A_n (r_0^n \pi) &= \frac{1}{n}\sum_{i=1}^{6} Q_i \int_0^{2\pi} H\Big[\theta - \frac{(i-1)\pi}{3}\Big]\cos(n\theta)d\theta \\
A_n &= \frac{-1}{r_0^n n\pi}\sum_{i=1}^{6} Q_i sin(i-1)\frac{n\pi}{3} \\
&= \frac{-1}{r_0^n n\pi}\Big[\sum_{i=1}^{5} Q_i \sin(i-1)\frac{n\pi}{3} + Q_6\Big] \\
&= \frac{-1}{r_0^n n\pi}\Big[\sum_{i=1}^{5} Q_i \sin(i-1)\frac{n\pi}{3} - \sum_{i=1}^{5} Q_i \sin\frac{5n\pi}{3}\Big] \\
&= \frac{-1}{r_0^n n\pi}\Big[\sum_{i=1}^{5} Q_i \Big[\sin(i-1)\frac{n\pi}{3} - \sin\frac{5n\pi}{3}\Big]\Big] \\
&= \frac{2}{r_0^n n\pi}\sum_{i=1}^{5} Q_i \sin\frac{(6-i)n\pi}{6}\cos\frac{(4+i)n\pi}{6}
\end{aligned}
$$

$$
\boxed{A_n = \frac{2}{r_0^n n\pi}\sum_{i=1}^{5} Q_i \sin(\frac{n(6-i)\pi}{6})\cos(\frac{n(4+i)\pi}{6})} \tag{A.9}
$$

Similar to the derivation for A_n, B_n can also be derived

$$
\boxed{B_n = \frac{2}{r_0^n n\pi}\sum_{i=1}^{5} Q_i \sin(\frac{n(6-i)\pi}{6})\sin(\frac{n(4+i)\pi}{6})} \tag{A.10}
$$

The solution for streamfunction in equation A.5 is now known since all the coefficients are known. The final solution looks like:

$$\psi = A_0 + \sum_{n=1}^{\infty} r^n [A_n \cos(n\theta) + B_n \sin(n\theta)]$$

$$A_0 = \frac{1}{6} \sum_{i=1}^{5} Q_i (6-i)$$

$$A_n = \frac{2}{r_0^n n\pi} \sum_{i=1}^{5} Q_i \sin(\frac{n(6-i)\pi}{6}) \cos(\frac{n(4+i)\pi}{6})$$

$$B_n = \frac{2}{r_0^n n\pi} \sum_{i=1}^{5} Q_i \sin(\frac{n(6-i)\pi}{6}) \sin(\frac{n(4+i)\pi}{6})$$

From this, velocity field can be derived as:

$$v_r = \frac{1}{r}\frac{\partial \psi}{\partial \theta} = \sum_{n=1}^{\infty} n r^{n-1} \Big[- A_n \sin(n\theta) + B_n \cos(n\theta) \Big] \tag{A.11}$$

$$v_\theta = -\frac{\partial \psi}{\partial r} = - \sum_{n=1}^{\infty} n r^{n-1} \Big[A_n \cos(n\theta) + B_n \sin(n\theta) \Big] \tag{A.12}$$

B

Appendix B

In this appendix, the pathlines traced by a single particle to form alphabets are shown. The sources and sinks follow the same colour code as in the chapters before.

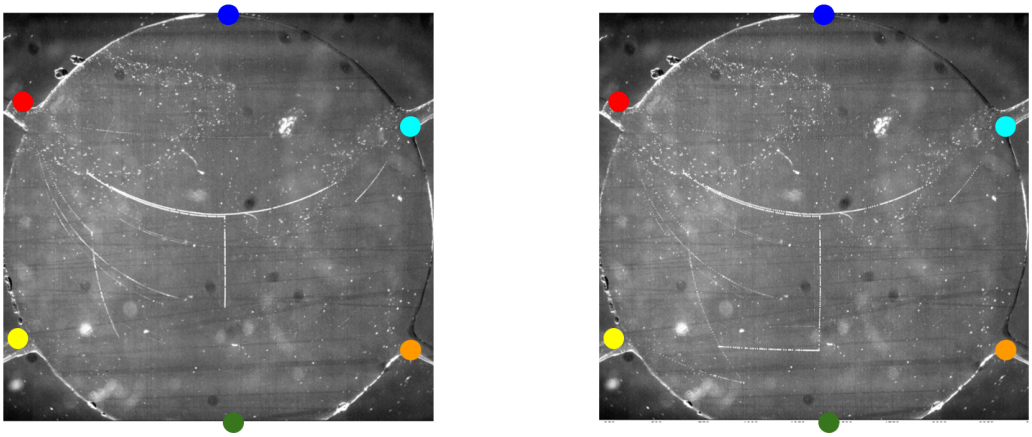

(a) Letter T

(b) Letter J

Figure B.1: Pathlines for particles tracing letters

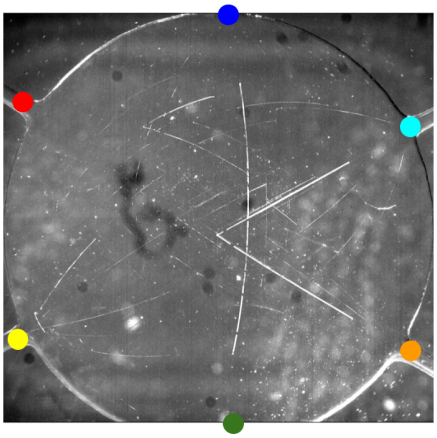

Figure B.2: Particle pathline for letter K

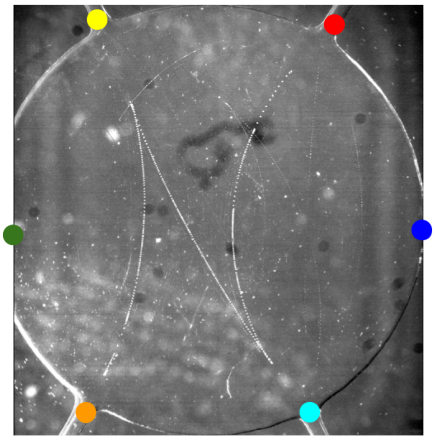

Figure B.3: Particle pathline for letter N

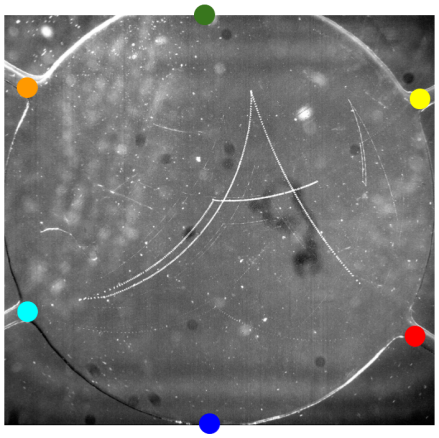

Figure B.4: Particle pathline for letter A

C

APPENDIX C

While writing an algorithm for manipulating particles, it becomes imperative to keep the flow rates within the range of the pump. Moreover, it is also necessary to keep the change in flow rates should as small as possible.

In this case, flow rates were prescribed as a function of time as shown in equation C.1. The initial and final position for the particle was set to values mentioned in equations C.2 and C.3.

$$Q_i(t) = \sum q_i^{(n)} L_n(t) \tag{C.1}$$

where,L_n represents the Legendre polynomials of degree n, $q_i^{(n)}$ is the coefficient for the i^{th} flow port and n^{th} degree Legendre polynomial.

$$\underline{X}(t=0) = \underline{X}_0 \tag{C.2}$$

$$\underline{X}(t=\tau) = \underline{X}_1 \tag{C.3}$$

where, τ represents the time that the particle should take to reach the final position.
First an unconstrained optimization is carried out using the *fminunc* function of MATLAB. The function to be minimized in this case is shown in equation C.4. This will ensure that the particle will reach the final position, but there are no constraints on the flow rates.

$$J = |\underline{X}(t=\tau)| - \underline{X}_1| \tag{C.4}$$

After the unconstrained optimization, the function to be minimized is changed to C.5 and is subject to the condition C.6

$$J = \alpha \int_0^\tau (\frac{dQ}{dt})^2 dt + \beta \int_0^\tau (\sum Q_i^2) dt \tag{C.5}$$

$$s.t. |\underline{X}(t=\tau)| - \underline{X}_1| = 0 \tag{C.6}$$